# อนุภาคระดับนาโนเมตรของทองคำที่ทำให้เสถียรด้วยพอลิเมอร์ที่ตอบสนองต่ออุณหภูมิสำหรับการตรวจหาโปรตีน

นางสาวกีรติ กุศลกรรมบถ

วิทยานิพนธ์นี้เป็นส่วนหนึ่งของการศึกษาตามหลักสูตรปริญญาวิทยาศาสตรมหาบัณฑิต
สาขาวิชาปิโตรเคมีและวิทยาศาสตร์พอลิเมอร์
คณะวิทยาศาสตร์ จุฬาลงกรณ์มหาวิทยาลัย
ปีการศึกษา 2554

# THERMORESPONSIVE POLYMER-STABILIZED GOLD NANOPARTICLES FOR PROTEIN DETECTION

Miss Keerati Kusolkamabot

A Thesis Submitted in Partial Fulfillment of the Requirements
for the Degree of Master of Science Program in Petrochemistry and Polymer Science
Faculty of Science
Chulalongkorn University
Academic Year 2011

| | |
|---|---|
| Thesis Title | THERMORESPONSIVE POLYMER-STABILIZED GOLD NANOPARTICLES FOR PROTEIN DETECTION |
| By | Miss Keereti Kusolkamabot |
| Field of Study | Petrochemistry and Polymer Science |
| Thesis Advisor | Associate Professor Voravee P. Hoven, Ph.D. |

---

Accepted by the Faculty of Science, Chulalongkorn University in Partial Fulfillment of the Requirements for the Master's Degree

……Dean of the Faculty of Science
(Professor Supot Hannongbua, Dr.rer.nat.)

THESIS COMMITTEE

……Chairman
(Associate Professor Supawan Tantayanon, Ph.D.)

……Thesis Advisor
(Associate Professor Voravee P. Hoven, Ph.D.)

……Examiner
(Assistant Professor Varawut Tangpasuthadol, Ph.D.)

……External Examiner
(Gamolwan Tumcharern, Ph.D.)

กีรติ กุศลกรรมบถ: อนุภาคระดับนาโนเมตรของทองคำที่ทำให้เสถียรด้วยพอลิเมอร์ที่ตอบสนองต่ออุณหภูมิสำหรับการตรวจหาโปรตีน. (THERMORESPONSIVE POLYMER-STABILIZED GOLD NANOPARTICLES FOR PROTEIN DETECTION) อ. ที่ปรึกษาวิทยานิพนธ์หลัก: รศ.ดร.วรวีร์ โฮเว่น, 69 หน้า.

เตรียมอนุภาคระดับนาโนเมตรของทองคำที่ถูกทำให้เสถียรด้วยพอลิเมอร์ที่ตอบสนองต่ออุณหภูมิโดยการตรึงพอลิ(*เอ็น*-ไอโซโพรพิลแอคริลาไมด์) ที่มีหมู่ปลายเป็นไทออล (สองน้ำหนักโมเลกุล คือ 6 และ 8 กิโลดาลตัน) บนอนุภาคระดับนาโนเมตรของทองคำที่ทำให้เสถียรด้วยซิเตรท การเปลี่ยนสีของสารละลายอนุภาคระดับนาโนเมตรของทองคำที่ทำให้เสถียรด้วยพอลิ(*เอ็น*-ไอโซโพรพิลแอคริลาไมด์) จากสีแดงเป็นสีม่วงอมสีน้ำเงิน โดยปราศจากการตกตะกอนเมื่อให้ความร้อนถึง 40 องศาเซลเซียส ซึ่งมีค่าสูงกว่าอุณหภูมิการละลายวิกฤติตอนล่างของ พอลิ(*เอ็น*-ไอโซโพรพิลแอคริลาไมด์) แสดงถึงสมบัติการตอบสนองต่ออุณหภูมิของอนุภาคระดับนาโนเมตรของทองคำที่สังเคราะห์ขึ้น ในงานวิจัยนี้นำอนุภาคระดับนาโนเมตรของทองคำที่ทำถูกให้เสถียรด้วยพอลิ(*เอ็น*-ไอโซโพรพิลแอคริลาไมด์) มาใช้ตรวจหาโปรตีนโดยใช้รูปแบบการเปลี่ยนแปลงสัญญาณที่แตกต่างกันและอาศัยการระงับสัญญาณฟลูออเรสเซนส์ของฟลูออโรฟอร์ด้วยอนุภาคระดับนาโนเมตรของทองคำ ในการตรวจวัดเมื่อเติมโปรตีนที่ต้องการตรวจวิเคราะห์ลงไป ฟลูออโรฟอร์ที่ถูกระงับสัญญาณฟลูอเรสเซนส์โดยอนุภาคระดับนาโนเมตรของทองคำจะจับกับโปรตีนและหลุดจากพื้นผิวของอนุภาคระดับนาโนเมตรของทองคำ ส่งผลให้ฟลูออโรฟอร์สามารถกลับมาให้สัญญาณฟลูออเรสเซนส์ได้อีกครั้งหนึ่ง ทั้งนี้สามารถพัฒนาการตรวจหาโปรตีนทั้งหกชนิดในรูปแบบแอเรย์ได้จากอนุภาคระดับนาโนเมตรของทองคำที่ทำให้เสถียรด้วยพอลิ(*เอ็น*-ไอโซโพรพิลแอคริลาไมด์) ที่มีน้ำหนักโมเลกุลและคอนฟอร์เมชันต่างกัน ร่วมกับการใช้ฟลูออโรฟอร์ชนิดจีศูนย์เด็นดริทิกเฟนิลีนเอทินิลีนที่มีประจุบวกของหมู่ไทรเมทิลแอมโมเนียม จากการวิเคราะห์ทางสถิติด้วยทฤษฎีวิเคราะห์การแยกแยะเชิงเส้นพบว่าสามารถจำแนกชนิดของโปรตีนด้วยความแม่นยำสูงถึงหนึ่งร้อยเปอร์เซ็นต์โดยใช้อนุภาคระดับนาโนเมตรของทองคำที่ทำถูกให้เสถียรด้วยพอลิ(*เอ็น*-ไอโซโพรพิลแอคริลาไมด์) เพียงสองชนิด

สาขาวิชา ปิโตรเคมีและวิทยาศาสตร์พอลิเมอร์ ลายมือชื่อนิสิต .....

ปีการศึกษา 2554 ลายมือชื่อ อ.ที่ปรึกษาวิทยานิพนธ์หลัก .....

# # 4972400123 : MAJOR PETROCHEMISTRY AND POLYMER SCIENCE
KEYWORDS: GOLD NANOPARTICLES / PNIPAM / FLUORESCENCE / PROTEIN / SENSOR

KEERATI KUSOLKAMABOT: THERMORESPONSIVE POLYMER-STABILIZED GOLD NANOPARTICLES FOR PROTEIN DETECTION. ADVISOR: ASSOC. PROF. VORAVEE P. HOVEN, Ph.D., 69 pp.

Gold nanoparticles stabilized by thermoresponsive polymer, poly(*N*-isopropylacrylamide) (PNIPAM-AuNPs), were prepared by surface grafting of thiol-terminated PNIPAM (having two targeted molecular weight 6 and 8 kDa) onto citrate-stabilized AuNPs. The color change of the PNIPAM-AuNPs solution from red to blue-purple without precipitation when the solution was heated to 40 ºC, above the lower critical solution temperature (LCST) of PNIPAM indicated the thermoresponsive property of the synthesized AuNPs. In this work, PNIPAM-AuNPs were used to detect proteins by chemical nose approach based on fluorescence quenching of fluorophore by AuNPs. In the detection, upon an addition of protein analyte, quenched fluorophore absorbed on the AuNPs surface can be attracted by protein and released from the AuNPs surface resulting in the recovery of fluorescence signal of the fluorophore. An array-based sensing platform for detection of six proteins can be developed from the PNIPAM-AuNPs having different molecular weight and conformation in combination with a G0 dendritic phenylene-ethynylene fluorophore having positively charged $N(CH_3)_3^+$ groups. From Linear Discriminant Analysis (LDA), it was found that 100% accuracy of protein classification can be achived by using only two types of PNIPAM-AuNPs.

Field of Study: Petrochemistry and Polymer Science Student' Signature .....

Academic Year: 2011 Advisor's Signature .....

# ACKNOWLEDGEMENTS

First and foremost I wish to express my sincere and deep gratitude to my advisor, Associate Professor Dr. Voravee P. Hoven for her thoughtful guidance, steady encouragement and support, and consistent generosity and consideration. Working with her has been the best course of my study. I would also like to thank all committee members, Associate Professor Dr. Supawan Tantayanon, Assistant Professor Dr.Varawut Tangpasuthadol and Dr. Gamolwan Tumcharern for their valuable suggestions and time to review the thesis.

I would really like to acknowledge Dr.Kanet Wongravee for his kind assistance with linear discriminant analysis. I am thankful to the friendly staff of Organic Synthesis Research Unit (OSRU), and all my friends, for their friendliness, helpful discussions, cheerful attitude and encouragements during my thesis work.

Finally, I also wish to especially thank my family members for their love, kindness and support throughout my entire study.

# CONTENTS

Page

Page

Page

# LIST OF TABLES

# LIST OF FIGURES

Figure Page

Figure Page

Figure Page

# LIST OF SCHEMES

Scheme Page

# LIST OF ABBREVIATIONS

| | |
|---|---|
| ACPA | : 4,4'-azobis(4-cyanopentanoic acid) |
| AFM | : Atomic force microscopy |
| BSA | : Bovine serum albumin |
| CTA | : Chain transfer agent |
| Con A | : Concanavalin A |
| CPD | : 4-Cyano-4-(thiobenzoylthio)pentanoic acid |
| ELISA | : Enzyme-linked immunosorbent assay |
| Fib | : Fibrinogen |
| FTIR | : Fourier transform infrared spectroscopy |
| FRET | : Fluorescence resonance energy transfer |
| GPC | : Gel-Permeation Chromatography |
| AuNPs | : Gold nanoparticles |
| PNIPAM-AuNPs | : AuNPs stabilized by PNIPAM monolayer |
| Hgb | : Hemoglobin |
| TF | : Holo-transferrin human |
| LCST | : Lower critical solution temperature |
| LDA | : Linear discriminate analysis |
| Lys | : Lysozyme |
| NMR | : Nuclear magnetic resonance spectroscopy |
| PBS | : Phosphate buffered saline |
| PCS | : Photon Correlation Spectroscopy |
| PAA | : Polyacrylic acid |
| PDMAEMA | : Poly(2-(Dimethylamino)ethyl methacrylate) |

| | |
|---|---|
| PNIPAM | : Poly(*N*-isopropylacrylamide) |
| PPE | : Poly(ρ-phenyleneethynylene) |
| RAFT | : Reversible addition-fragmentation chain transfer |
| SEM | : Scanning Electron Microscopy |
| SERS | : Surface-enhanced raman scattering |
| SPR | : Surface Plasmon resonance |
| $NaBH_4$ | : Sodium borohydride |
| NaOH | : Sodium hydroxide |
| TEM | : Transmission electron microscopy |
| TCEP | : Tris(2-carboxyethyl)phosphine hydrochloride |
| UV | : Ultraviolet |
| ζ-potential | : Zeta-potential |

# CHAPTER I

# INTRODUCTION

## 1.1 Statement of Problem

Gold nanoparticles (AuNPs) have been a focus of considerable interest because of their potential applications for catalysis, diagnosis, and photoelectronic devices. Highly dispersed AuNPs solutions exhibit a red color with an absorption band around 520 nm due to the excitation of surface plasmon by incident light. The association of the AuNPs in the dispersed solution induces a color change from red to blue-purple, which would be applied to colloidal sensors [1,2,3]. However, the AuNPs in solution are susceptible to aggregation themselves. To improve their dispersibility, the AuNPs may be coated with a water-soluble polymer having a functionality that can react with gold.

Polymers prepared by reversible addition-fragmentation chain transfer (RAFT) polymerization with use of a dithioester chain transfer agent have a well-controlled molecular weight and narrow molecular weight distribution. Another advantage of the RAFT polymerization is that polymers bearing dithioester groups at the chain ends can be obtained. The terminal dithioester group can be converted to a thiol terminated functionality, which can be used for various reactions including grafting onto the surface of gold.

It is well known that an aqueous solution of poly(*N*-isopropylacrylamide) (PNIPAM) undergoes a thermally reversible phase separation [4]. PNIPAM dissolves in water assuming a random coil conformation at room temperature, but it separates from the aqueous phase when heated above 31-32 °C, a lower critical solution temperature (LCST). Recently, well-defined PNIPAM has been synthesized by RAFT polymerization by several research groups [5,6,7,8,9]. As reported by Zhu *et al.*, thiol-terminated PNIPAM prepared by RAFT polymerization can be grafted on AuNPs. The 13-nm AuNPs coated with thiol-terminated PNIPAM showed thermoresponsive behavior which was revealed by a sharp clear-to-opaque transition in water between 25 and 30 °C [10]. More detailed reports on the preparation and thermoresponsive

behavior of PNIPAM-coated AuNPs were also described by Tenhu and co-workers [11,12,13].

Recently, it has been reported that protein as a biomarker can be detected by chemical nose approach based on fluorescence quenching of fluorophore by functionalized AuNPs. The binding equilibrium between fluorophore and AuNPs would be altered because of competitive binding of protein analyte. Upon an addition of protein analyte, quenched fluorophore adsorbed on the AuNPs surface can be replaced by protein resulting in the recovery of fluorescence signal from the fluorophore. The fluorescence response can be positive or negative depending on the binding affinity of protein towards AuNPs and fluorophore. Although the chemical nose approach relies very much on non-specific interactions between protein and AuNPs, it is selective enough to be used for identifying the type of individual protein based on the variation of quenching ability of AuNPs having different functionality and the binding strength between the functionalized AuNPs and different kind of protein [14].

Although there are a few literatures describing the synthesis of AuNPs using PNIPAM as the stabilizing agent, none of them have combined the thermoresponsive behavior of PNIPAM and the fluorescence quenching properties of AuNPs to create hybrid materials to be used for protein detection. Their biosensing applications, in particular, have not yet been mentioned. Herein, a biosensor which prepared by thermoresponsive AuNPs is reported.

In this work, AuNPs stabilized by PNIPAM (PNIPAM-AuNPs) were prepared by surface grafting of thiol-terminated PNIPAM synthesized by RAFT polymerization onto citrate-stabilized AuNPs. By changing the PNIPAM thickness and conformation which can be varied as a function of molecular weight and temperature, 4 different types of PNIPAM-AuNPs (NP1-NP4) were generated (**Figure 1.1**). Together with the G0 dendritic phenylene-ethynylene fluorophore having 3 positively charged $N(CH_3)_3^+$ groups per molecule, an array-based sensing platform for protein detection was developed based on the concept of fluorescence quenching as mentioned above (**Figure 1.2**). In addition, the AuNPs stabilized by mixed monolayers of PNIPAM and polymers having negatively (NP5) or positively (NP6) charges were also prepared (**Figure 1.3**). We expected that the charge variation of AuNPs should have some impact on the detection efficiency.

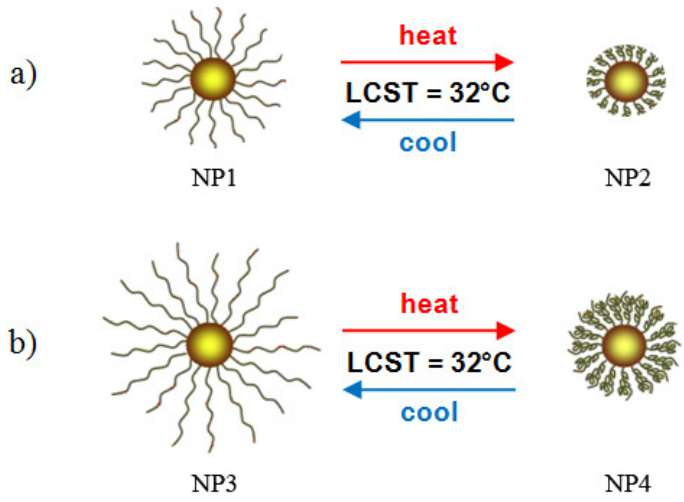


**Figure 1.1** Thermoresponsive behavior of a) low molecular weight PNIPAM-stabilized AuNPs and b) high molecular weight PNIPAM-stabilized AuNPs before and after heat treatment above LCST that yielded 4 different types of PNIPAM-AuNPs (NP1-NP4).

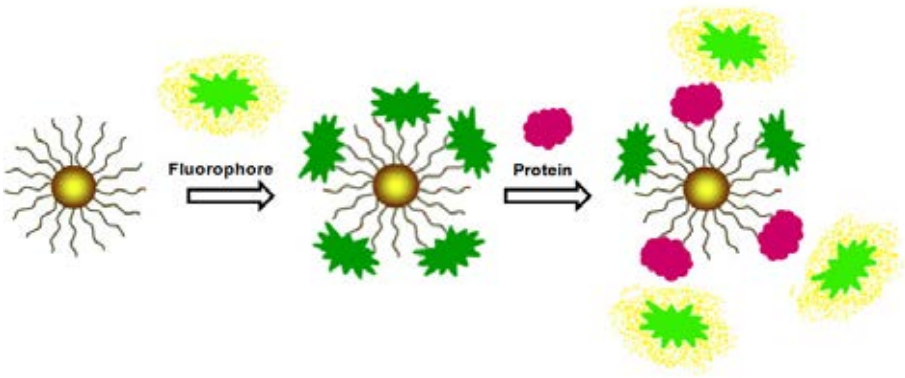


**Figure 1.2** Schematic representation demonstrating the concept used for developing a sensor based on competitive binding of protein and fluorophore with AuNPs that has impact on fluorescence quenching.

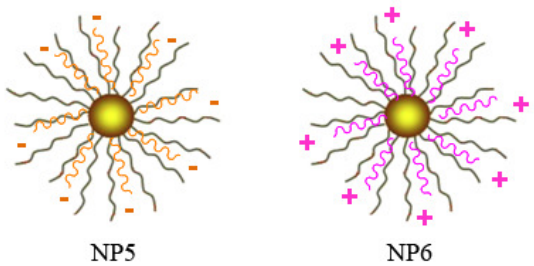


**Figure 1.3** Chemical structures of AuNPs stabilized by mixed monolayers of PNIPAM and polymers having negatively (NP5) or positively (NP6) charges.

## 1.2 Objectives

1. To synthesize and characterize PNIPAM-AuNPs
2. To test thermoresponsive behavior of the synthesized PNIPAM-AuNPs
3. To develop a protein detection method based on fluorescence quenching of fluorophore by PNIPAM-AuNPs

## 1.3 Scope of Investigation

The stepwise investigation was carried out as follows:

1. Literature survey for related research work
2. Synthesis and characterization of thiol-terminated PNIPAM
3. Synthesis and characterization of AuNPs stabilized by PNIPAM monolayer via two methods.
   3.1 Using grafting-to method
   3.2 Using grafting-from method
4. Synthesis and characterization of thiol-terminated PAA and thiol-terminated QPAMAEMA
5. Synthesis and characterization of AuNPs stabilized by mixed monolayers of PNIPAM and PAA or PNIPAM and QPDMAEMA via grafting-to method.
6. To evaluate the applicability of the synthesized AuNPs for protein detection

# CHAPTER II

# THEORY AND LITERATURE REVIEW

## 2.1 Gold Nanoparticles and Their Properties

Gold nanoparticles (AuNPs) is a suspension of nanometer-sized (1-100 nm) particles of gold in a fluid [15]. As shown in **Figure 2.1**, the particles may have a variety of size, shape and conformation.

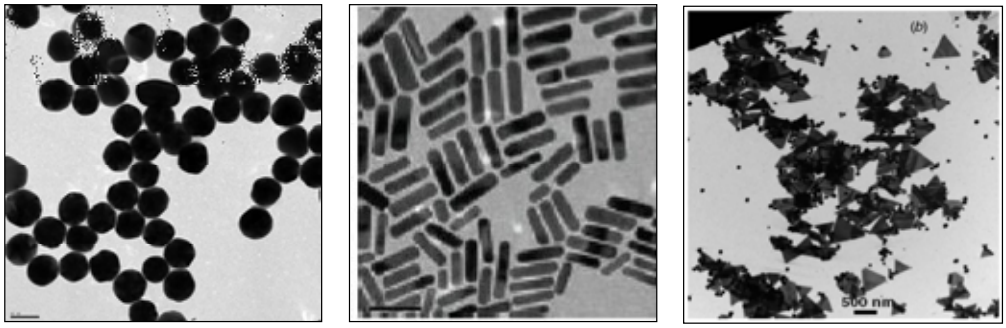


(a) (b) (c)

**Figure 2.1** Different shapes of AuNPs: (a) gold nanoparticles, (b) gold nanorods [16], and (c) gold nanotriangles [17].

At this nanoscale, the AuNPs provide large surface to volume ratio, physical and chemical properties of them are thus unique and very different from both the bulk and the constituent atoms or molecules, most obvious example being the color change from yellow to ruby red when bulk gold is converted into nanoparticulate gold [18]. This ruby red color of the AuNPs is due to the presence of a plasmon absorption band. This absorption band occurs when the incident photon frequency is in resonance with the collective excitation of the conductive electrons of the particle. This effect was termed localized surface plasmon resonance (LSPR) which has an absorption band in the visible region at 530-540 nm. It is well-known that the association of the AuNPs in the dispersed solution induces a color change from red to blue-purple and gives rise to a red shift in the absorption band (**Figure 2.2**), which would be applied to many applications. Some examples include optical devices, chemical, and biological sensors.

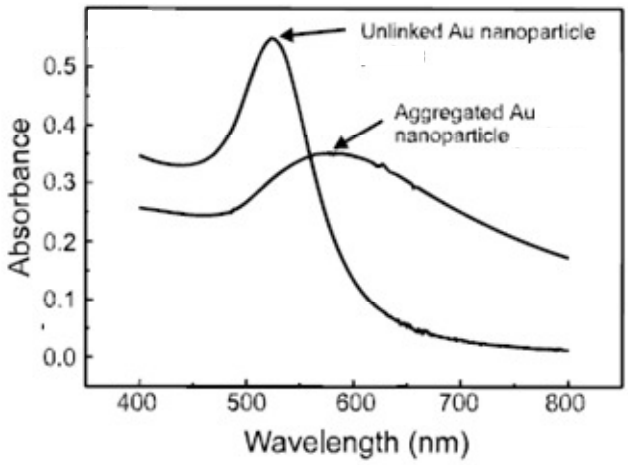


**Figure 2.2** Absorption band of unlinked and aggregated AuNPs [19].

In biological applications, AuNPs are the popular materials because AuNPs can be synthesized in a direct manner and can be made highly stable with excellent biocompatibility using appropriate ligands [20]. The AuNPs properties can be tuned by varying their size, shape, and chemical surrounding environment. For example, the binding event between recognition element and the analyte can alter physicochemical properties of transducer AuNPs, such as plasmon resonance absorption, conductivity, etc., that in turn can generate a detectable response signal (**Figure 2.3**). Finally, AuNPs offer a suitable platform for multi-functionalization with a wide range of organic or biological ligands for the selective binding and detection of small molecules and biological targets [21,22,23].

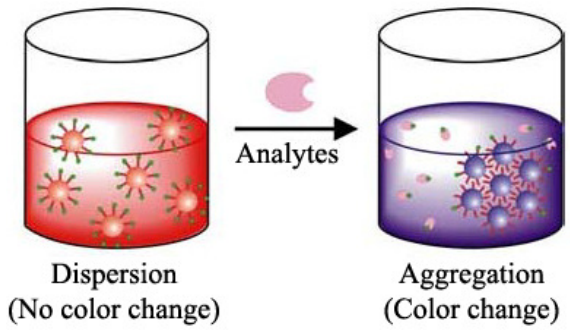


**Figure 2.3** AuNPs based biosensor. The color of aqueous solution changes during analytes-induced AuNPs aggregation.

## 2.2 Preparation of Gold Nanoparticles and Their Surface Funtionalization

Numerous preparative methods for AuNPs have been reported. Considerable effort has been devoted to synthesis of AuNPs, focusing on control over their size, shape, solubility, stability, and functionality.

In 1951, Turkevich *et al.* developed one of the most popular approaches for the synthesis of AuNPs, using citrate reduction of $HAuCl_4$ in water. In this method, citric acid acts as both reducing and stabilizing agent and provides AuNPs with diameters of 20 nm. This method is often used even now when a rather loose shell of ligand are required around the gold core in order to prepare a precursor to valuable AuNPs-based materials [24].

Surfactants and polymers, are also used as stabilizer to control the particle size, prevent aggregation, and introduce functionality to particle surfaces. In the case of polymers, they can usually act as stabilizing agent or as both reducing and stabilizing agent. It has been reported that polymers are effective stabilizing agent for AuNPs because they are able to combine both electrostatic and steric stabilizations.

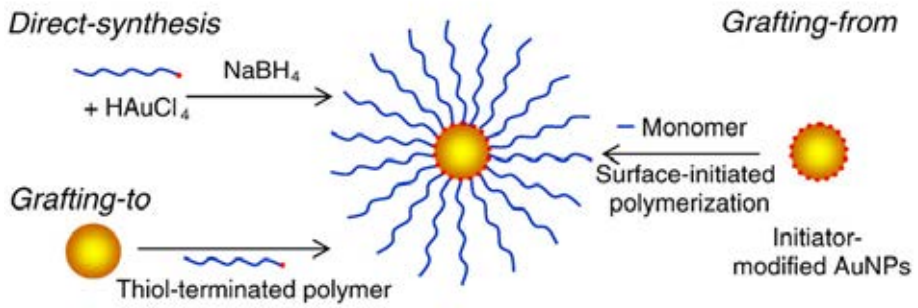


**Scheme 2.1** Main preparative approaches for the intelligent polymer stabilized-AuNPs based on the covalent linkages.

The strategies widely used for creating polymer-stabilized AuNPs are "direct-synthesis" by "grafting-to" or "grafting-from" (**Scheme 2.1**). For direct synthetic method, $HAuCl_4$ can be directly reduced by reducing agents in the presence of sulfur-terminated polymers and directly formed metal nanoparticles [25,26]. The grafting-from method consists of polymer chain growth from small initiators attached to AuNPs [27,28,29]. This technique provides a very dense polymer brushes. Frequently used methods include reversible addition-fragmentation chain transfer (RAFT)

polymerization [30] and surface- initiated atom-transfer radical polymerization (SI-ATRP) [31,32]. Grafting-to method enables one-pot synthesis of AuNPs stabilized by thiol-terminated polymers [33,34,35,36], and generally produces a sparse coverage. The polymer chains grafted on AuNPs surface cannot only enhance the stability of gold cores, but also provide functionality to the gold shell which may possess different properties depending on the physical and chemical characteristics of the grafted polymer.

Intelligent polymers are also known as "stimuli-responsive" or "environmentally sensitive" polymers [37,38,39,40], which will undergo relatively large and abrupt, physical or chemical changes as responses to small external stimuli in the environmental conditions [41,42,43,44]. Poly(*N*-isopropylacrylamide) (PNIPAM), one of the most popular thermoresponsive polymers, has been widely studied due to the reversibly responsive features. The thermal response of the polymer chains can be ascribed to the polymer solubility in different environments. For instance, water is a good solvent for the PNIPAM below the lower critical solution temperature (LCST, 32°C). In this case, the polymer chains are hydrated and adopt a random coiled conformation. Water becomes a poor solvent above 32 °C and thereby the polymer chains are dehydrated and turn into a globular conformation (**Figure 2.4**) [45,46,47].

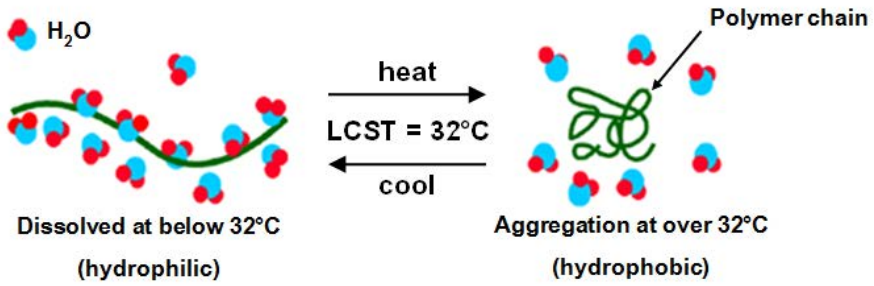


**Figure 2.4** Responsive property of the thermoresponsive polymer.

Such conformational transition of the PNIPAM chains results in a rapid hydrophilic to hydrophobic change in aqueous solution, so the phase separation occurs due to the thermoresponsive property. When the PNIPAM chains were immobilized onto a solid surface, the thermoresponsive phase transition from hydrophilic to hydrophobic should make the polymer collapse into the solid surface, which can schematically be illustrated in **Figure 2.5**.

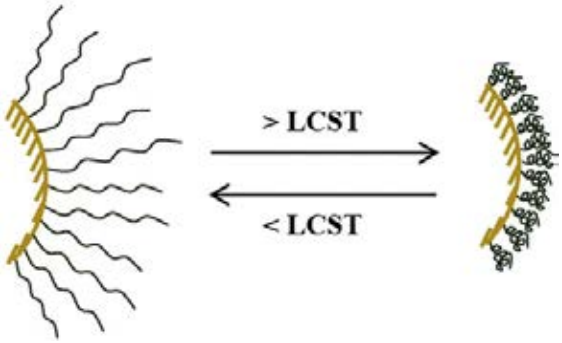


**Figure 2.5** Responsive conformational change of the PNIPAM chains on AuNPs surface.

In 2003, Raula, *et al.* [11] focused on the synthesis of AuNPs protected by PNIPAM. The polymerization of NIPAM was initiated from the surface of AuNPs modified with 4-cyanopentanoic acid dithiobenzoate (CPD) by RAFT polymerization. The number mean diameter of the AuNPs core was 3.2 nm. The molar mass of the PNIPAM ligand was 21,000 g/mol. The changes in the surface plasmon of gold were investigated in different media, and as a function of particle concentration, as well as of temperature in aqueous solutions. The particles were soluble slightly in water, forming aggregates. The area and the maximum wavelength of the plasmon band in water decreased with dilution and increasing temperature.

In 2004, Zhu, *et al.* [10] reported the synthesis of AuNPs coated with thiol-terminated PNIPAM prepared by RAFT polymerization. PNIPAM-stabilized AuNPs showed uniform size distribution (13 nm) and potential long-term stability. The thermoresponsive AuNPs was realized by a sharp clear-to-opaque transition in water between 25 and 30 °C.

In 2007, Yusa, *et al.* [48] prepared thermoresponsive AuNPs via grafting-to method. Thiol-terminated PNIPAM (PNIPAM-SH) was prepared by RAFT polymerization. They found that the color of PNIPAM-AuNPs in pure water was pink independent of the temperature while the thermoresponsive behavior was found to be sensitively affected by added salt. In 50 mM NaCl aqueous solution, the plasmon band at 40 °C was red shifted compared with that at 25 °C because of interparticle associations. Furthermore, this thermoresponsive property observed for the salt-containing solutions was completely reversible.

In 2010, Chakraborty, *et al.* [49] synthesized thermoresponsive polymer brushes of PNIPAM on 20 nm colloidal gold. PNIPAM was grown from the surface of AuNPs with the help of 2-bromopropionyl bromide as the initiator. The polymerization reaction was carried out at room temperature under inert atmosphere and aqueous conditions. The system was found to exhibit thermoresponsive behavior above and below the LCST. The change in color was evident after 1 h of exposure to the 40 °C environment.

## 2.3 Gold Nanoparticles in Biological Applications

Many disease states are often associated with the presence of certain biomarker proteins or irregular protein concentrations. In biological application, AuNPs are the popular materials that are used in immunoassay. Immunoassays are tests that use antibody and antigen complexes (also called immunocomplexes) to measure the presence of a specific analyte in a sample. This property of highly specific molecular recognition of antigens by antibodies leads to high selectivity of assays. For example, immunoagglutination, an antibody (or antigen) is coated on the surface of AuNPs. When a sample containing the specific antigen (or antibody) is mixed with AuNPs solution, it causes the aggregation of AuNPs because one molecule of antigen (or antibody) can bind two antibodies, and the dielectric constant around the particle is changed (**Figure 2.6**). Aggregation of AuNPs changes the particle size, so the optical property of AuNPs also changes because this property depends on the size of particles. The change in optical property is proportional to the analyte concentration [50,51,52].

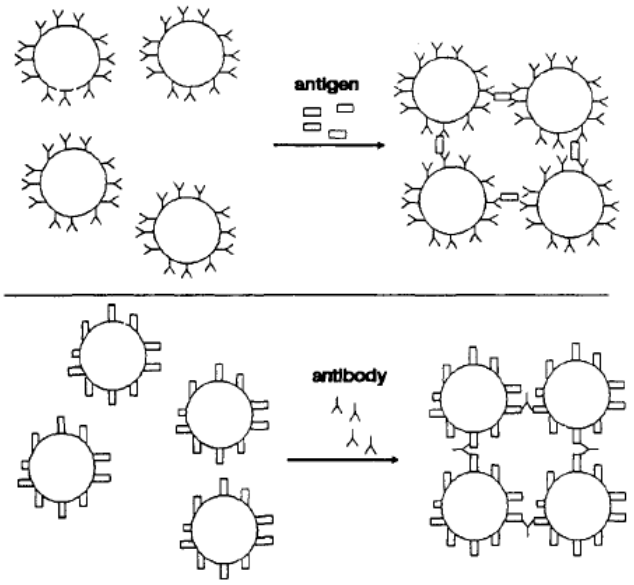


**Figure 2.6** Diagram of the aggregation of antibody-coated AuNPs by antigen (upper) and of antigen-coated AuNPs by antibody (lower).

In 2008, Du, *et al.* [53] developed the homogenous noncompetitive immunoassay based on the aggregation of antibody-functionalized AuNPs by the immunoreaction coupled with light scattering technique. This study found that the light scattering background of the suspensions of gold nanoparticles coated with antibodies is very low. The great enhancement of light scattering originated from the aggregate formation by the immunoreaction can be observed when micro amounts of the antigens were directly mixed with the gold nanoparticles. The proposed immunoassay can be performed with one-step operation in homogeneous solution within 10 min and the light scattering can be easily measured by using a common spectrofluorimeter. By using human immunoglobulin G (IgG) as a model analyte, a wide dynamic range of 0.05–10 μg/mL was achieved and as low as 10 ng/mL human IgG can be detected. The proposed immunoassay has been successfully applied to the determination of human IgG in serum samples, in which the results are well consistent with those of the enzyme-linked immunosorbent assay (ELISA), indicating its high selectivity and practicality.

In 2008, Chen, *et al.* [54] presented an alternative approach for aggregation-based immunoassays using Raman reporter-labeled immunogold nanoparticles as

probes coupled with surface-enhanced raman scattering (SERS) detection. AuNPs were functionalized with Raman reporter and antibody successively in a two-step process before the detection of target (**Figure 2.7A**). When the antigen was introduced, aggregation of AuNPs was induced by the immunoreaction between the antigen and the antibody modified on the surface of nanoparticles (**Figure 2.7B**). As a result, SERS signals of the reporter on the surface of AuNPs would be greatly enhanced. Therefore, the content of human IgG could be directly determined by measuring the Raman signal of the reporter. In addition, the process of aggregation was also investigated by TEM and UV–Vis absorption spectroscopy. Utilizing human IgG as a model protein, SERS response linearly correlated with the logarithmic concentration of the target over a range from 0.1 to 15 μg/mL with a detection limit of 0.1 μg/mL.

(A) Preparation of Raman reporter-labeled immunogold nanoparticles

(B) Immunoassay protocol

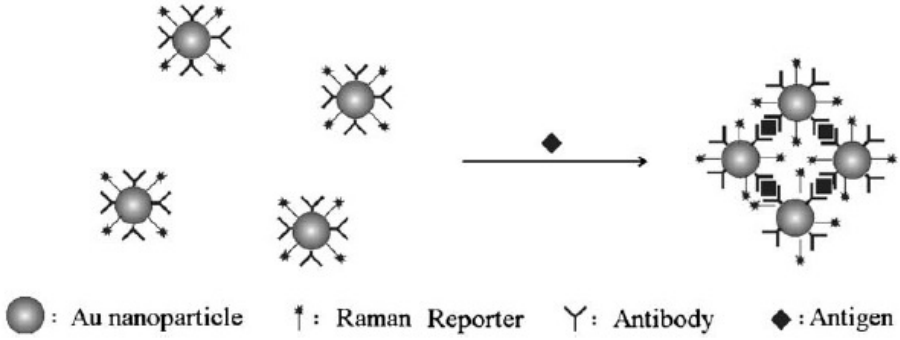


**Figure 2.7** Procedure for (A) preparation of Raman reporter-labeled immunogold nanoparticles and (B) immunoassay protocol.

Fluorescence resonance energy transfer (FRET) is a nonradiative process whereby an excited state donor D (usually a fluorophore) transfers energy to a proximal ground state acceptor A through long-range dipole-dipole interactions (**Figure 2.6**). The spectra show the absorption (Abs) and emission (Em) profiles of donor and acceptor. The acceptor must absorb energy at the emission wavelength of the donor, but does not

necessarily have to emit the energy fluorescently itself (i.e. dark quenching). The rate of energy transfer is highly dependent on many factors, such as the extent of spectral overlap, the relative orientation of the transition dipoles, and most importantly, the distance between the donor and acceptor molecules.

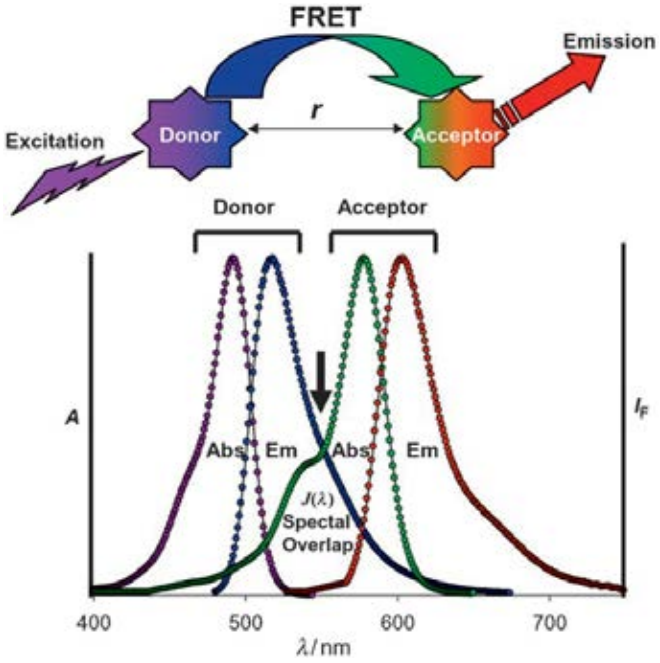


**Figure 2.8** Schematic representation of the FRET process.

AuNPs are increasingly used in FRET-based applications, mostly because of their exceptional quenching ability. Besides standard FRET considerations, the size and shape of the AuNPs also play an important role in FRET systems.

In 2005, Dulkeith, *et al.* [55] characterized the fluorescence quenching of dyes attached at a fix distance from the surface of various size AuNPs (1-30 nm) as well as dyes attached at varying distances (2-16 nm) from the surface of 6 nm AuNPs. Almost all the AuNPs were found not only to increase the nonradiative rate of decay of the dye, but also to decrease the radiative rate. Even 1 nm AuNPs were capable of to provide quenching efficiency of greater than 99%

However, all above immunoassays employ specific interactions. Array-based sensing, that is based on a concept of “chemical nose/tongue” strategies provide a useful alternative that uses differential selective interactions to generate patterns that can be used to identify analytes or changes in complex mixtures [56].

In 2007, Rotello, *et al.* [57] have developed a protein sensor using chemical nose technology. The prototype sensor array was generated using six cationic AuNPs of differing structures and ionic poly(ρ-phenyleneethynylene) (PPE) polymer. As illustrated in **Figure 2.9a**, electrostatic complexation of AuNPs and polymer results in fluorescence quenching of the polymer (fluorescence "OFF") through energy transfer. Addition of protein analytes then disrupts the quenched polymer-AuNPs complexes via competitive binding, causing fluorescence recovery of the polymer (fluorescence "ON"). The protein-nanoparticle interactions are differential [58], leading to a fingerprint fluorescence response pattern for individual proteins (**Figure 2.9b**) that was characterized using linear discriminate analysis (LDA). By employing the same principle, a AuNP-green fluorescent protein construct was used to detect and identify proteins at 500 nm in undiluted human serum (~1 mM overall protein concentration).

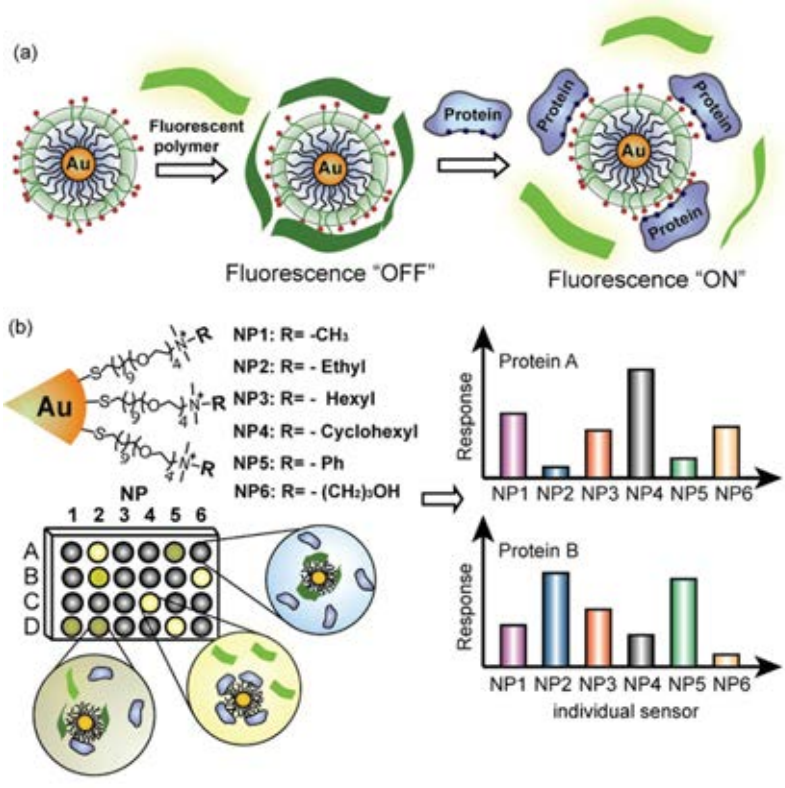


**Figure 2.9** Schematic illustration of "chemical nose" sensor array based on AuNP-fluorescent polymer/GFP conjugates. (a) The competitive binding between protein and quenched polymer-AuNP complexes leads to the restoration of fluorescence and (b) The combination of an array of sensors generates fingerprint response patterns for individual proteins [59].

In 2008, Phillips, *et al.* [60] used polymer-conjugated AuNPs to detect and identify bacteria. The cationic AuNPs and one anionic PPE polymer were used to generate sensor. Presence of bacteria disrupts the initially quenched assemblies leading to fluorescence restoration of PPE. From the distinct fluorescence response patterns, the sensor array was capable of identifying 12 bacteria (**Figure 2.10**).

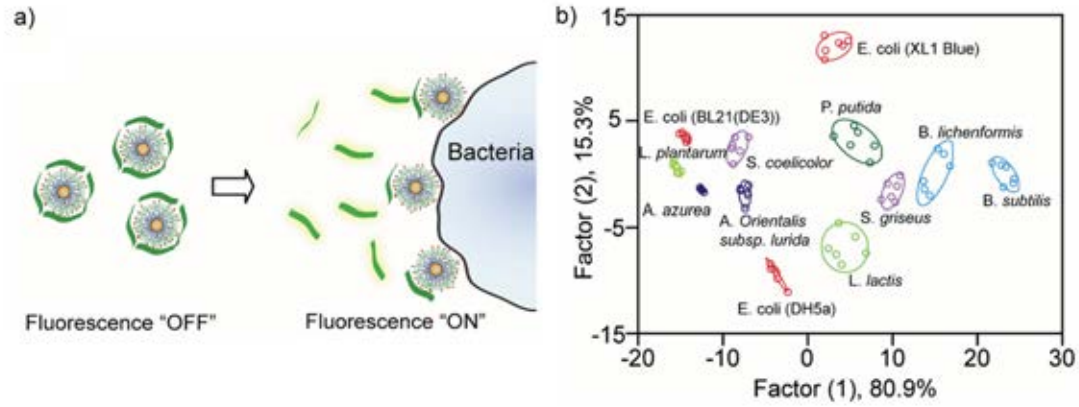


**Figure 2.10** Array-based sensing of bacteria: (a) Displacement assay between bacteria and the PEE-AuNPs complex, (b) Conical score plot of simplified fluorescence response patterns obtained with NP-PPE assembly arrays against bacteria.

# CHAPTER III
# EXPERIMENTAL

## 3.1 Materials

Hydrogen tetrachloroaurate ($HAuCl_4.3H_2O$), 4,4'-azobis(4-cyanopentanoic acid) (ACPA), 4-cyano-4-(thiobenzoylthio)pentanoic acid (CPD), tris(2-carboxyethyl)phosphine hydrochloride (TCEP), *N*-isopropylacrylamide (NIPAM), acrylic acid (AA), and 2-(dimethylamino)ethyl methacrylate (DMAEMA) were obtained from Aidrich (USA). Bovine serum albumin (BSA), lysozyme (Lys), fibrinogen (Fib), concanavalin A (Con A), hemoglobin (Hgb), holo-transferrin human (TF), dialysis bag (cut-off molecular weight of 12,400, and 3,500 g/mol), and phosphate buffered saline pH 7.4 (PBS) were bought from Sigma (USA). Lithium aluminium hydride solution ($LiAlH_4$), Sodium iodide (NaI), 2-ethanolamine, and tri-sodium citrate dihydrate ($Na_3C_6H_5O_7.2H_2O$) were obtained from Fluka (Switzerland). Methyl iodide ($CH_3I$) was purchased from Riedel-de Haen (Germany). Sodium hydroxide (NaOH), and 1,4-dioxane was bought from Carlo Erba (Italy). Tetrahydrofuran (THF) was bought from RCL Labscan. Methanol (MeOH), and sodium chloride (NaCl) were purchased from Merck (Germany). The above chemicals were analytical grade and used as received without further purification except NIPAM which was recrystallized in a mixture of benzene and *n*-hexane (3:7, v/v). AA was purified by distillation. DMAEMA was purified by filtered through a neutral $Al_2O_3$ column. Furthermore, four fluorophores (G0 dendritic phenylene-ethynylene fluorophore) having different charges synthesized by Dr.Nakorn Niamnont were provided by Associate Professor Dr. Mongkol Sukwattanasinit. All solutions were made using ultrapure distilled water that was obtained after purification using a Millipore Milli-Q system (USA) that involves reverse osmosis , ion exchange, and a filtration step (18.2 MΩ cm resistance).

## 3.2 Equipments

### 3.2.1 Nuclear Magnetic Resonance Spectroscopy (NMR)

The $^{1}H$ NMR spectra were recorded in $CF_3COOH/D_2O$ using Varian, model Mercury-400 nuclear magnetic resonance spectrometer (USA) operating at 400 MHz. Chemical shifts (δ) were reported in part per million (ppm) relative to tetramethylsilane (TMS) or using the residual protonated solvent signal as a reference.

### 3.2.2 Fourier Transform Infrared Spectroscopy (FT-IR)

The FT-IR spectra were recorded in KBr discs with a FT-IR spectrometer (Nicolet, USA), model Impact 410, with 32 scans at resolution 4 $cm^{-1}$. A frequency of 400-4000 $cm^{-1}$ was collected by using TGS detector.

### 3.2.3 Gel-Permeation Chromatography (GPC)

Molecular weight of synthesized polymer were analyzed by GPC using Waters 600 controller chromatograph equipped with HR1 and HR4 columns (Waters, MW resolving range = 100-500,000) at 35 °C and refractive index detector (Waters 2414). THF was used as an eluent with the flow rate of 1.0 mL/min. Sample injection volume was 50 µL. Five polystyrene standards (996-188,000 Da) were used for generating a calibration curve.

### 3.2.4 UV-Visible Spectroscopy

UV-Vis absorption spectra of AuNPs were obtained by CARY 100 Bio UV-visible spectrophotometer (Varian Ltd., USA). The scanning wavelength was from 200 to 800 nm.

### 3.2.5 Luminescence Spectrometer

Fluorescent signal of fluorophores were obtained by Perkin Elmer precisely (LS 45) luminescence spectrometer (PerkinElmer Inc., UK). The scanning wavelength was in a range of 400-700 nm.

### 3.2.6 Atomic Force Microscopy (AFM)

The presence of the polymer around the AuNPs was confirmed by a Seiko SPA 400 atomic force microscope (SII Nanotechnology Inc., Japan). The samples were prepared by dropping the AuNPs solution on a cleaned silicon wafer and dried by vacuum for 12 h prior to analysis. Measurements were performed in air at ambient temperature using tapping mode and silicon tips with a resonance frequency of 115-190 kHz.

### 3.2.7 Surface Plasmon Resonance (SPR)

SPR measurements used for the determination of polymer coverage on gold surface were conducted using a double channel, AutoLab ESPR (Eco Chemie, The Netherlands) at Scientific and technological Research Equipment Centre, Chulalongkorn University (Thailand).

### 3.2.8 Transmission Electron Microscopy (TEM)

The morphology and actual size of particles were analyzed by a JEOL JEM-2010 transmission electron microscopy (Japan) operating at 200 keV. The TEM samples were prepared by dropping approximately 10 μL of AuNPs solution on the carbon-coated copper grid and dried in a dessicator before analysis. The average diameters were reported from measurements of 30 random particles for each sample using Semafore software.

### 3.2.9 Scanning Electron Microscopy (SEM)

The size and the morphology of particles were determined by scanning electron microscope (SEM, Model JEOL JSM-6480LV). The average diameter of particles was calculated by measurement of 100 random particles using Semafore software.

### 3.2.10 Photon Correlation Spectroscopy (PCS)

The hydrodynamic size and zeta-potential ($\zeta$) of particles were determined using Nanosizer Nano-ZS (Malvern Instruments, UK). The solutions of AuNPs (1 mL) were sonicated for 3 min before measurement. The analysis was performed at 25°C using a scattering angle of 173°. All data are displayed as the mean $\pm$ standard deviation and are derived from at least three independent experiments. The data were calculated using the Helmholtz-Smoluchowski equation.

## 3.3 Preparation of Polymer-stabilized AuNPs by Grafting-to Technique

### 3.3.1 Synthesis of Thiol-terminated PNIPAM (PNIPAM-SH)

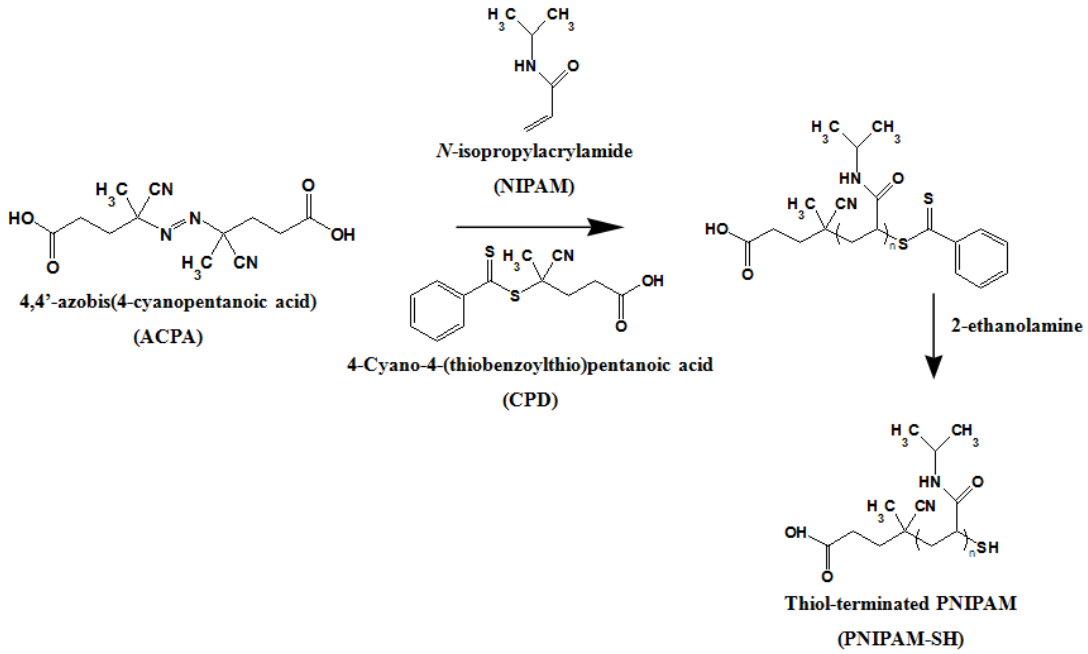


**Scheme 3.1** Synthesis of PNIPAM-SH by RAFT polymerization.

PNIPAM having two different target degree of polymerization (DP = 40 and 70) were prepared by RAFT polymerization. According to a method modified from that of Yusa *et al*. [48], CPD (17.5 mg, $6.25 \times 10^{-5}$ mol) and ACPA (8.8 mg, $3.13 \times 10^{-5}$ mol) were added to the NIPAM (565.8 mg, $500.00 \times 10^{-5}$ mol) solution in 1,4-dioxane (5 mL). The solution was degassed by purging with nitrogen gas for 30 min, and then heated at 70 °C for 24 h. After being cooled down in an ice bath, the reaction mixture was dialyzed against DI water at 4 °C for 3 days, before the PNIPAM was recovered by lyophilization. To remove the terminal dithiobenzoate group, an aqueous solution of PNIPAM was treated with 2-ethanolamine (30 mol equivalent of PNIPAM) and a trace amount (3-5 mg) of tris(2-carboxyethyl)phosphine hydrochloride (TCEP) at 25 $^{o}$C for 24 h. The solution was dialyzed against DI water at 4 $^{o}$C for 3 days. The PNIPAM-SH was then obtained after lyophilization. (The condition above was used to prepare PNIPAM DP=40. To prepare PNIPAM with DP of 70, CPD (11.1 mg, $3.97 \times 10^{-5}$ mol) and ACPA (4.5 mg, $1.59 \times 10^{-5}$ mol) were used instead.

### 3.3.2 Synthesis of Thiol-terminated PAA (PAA-SH)

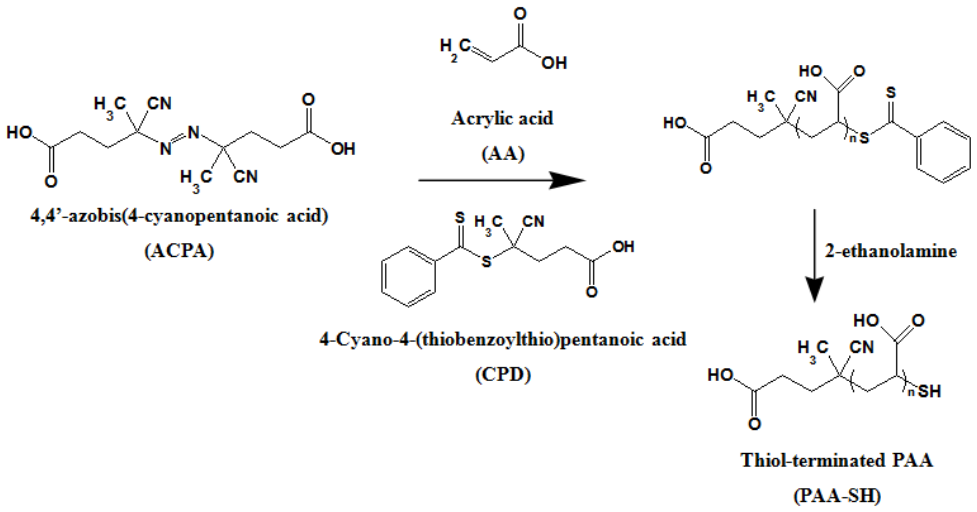


**Scheme 3.2** Synthesis of PAA-SH by RAFT polymerization.

CPD (31.1 mg, $11.13 \times 10^{-5}$) and ACPA (7.8 mg, $2.78 \times 10^{-5}$ mol) were added to the AA (686 µl, $1000.00 \times 10^{-5}$ mol) in 20 mL of PBS solution. The solution was degassed by purging with nitrogen gas for 30 min, and then heated at 70 °C for 20 h. After being cooled down in an ice bath, the reaction mixture was dialyzed against DI water at ambient temperature for 3 days, before the PAA was recovered by lyophilization. To remove the terminal dithiobenzoate group, an aqueous solution of PAA was treated with 2-ethanolamine (30 mol equivalent of PAA) and a trace amount of TCEP (3-5 mg) at ambient temperature for 24 h. The solution was dialyzed against DI water at ambient temperature for 3 days. The PAA-SH was then obtained after lyophilization.

### 3.3.3 Synthesis of Thiol-terminated QPDMAEMA (QPDMAEMA-SH)

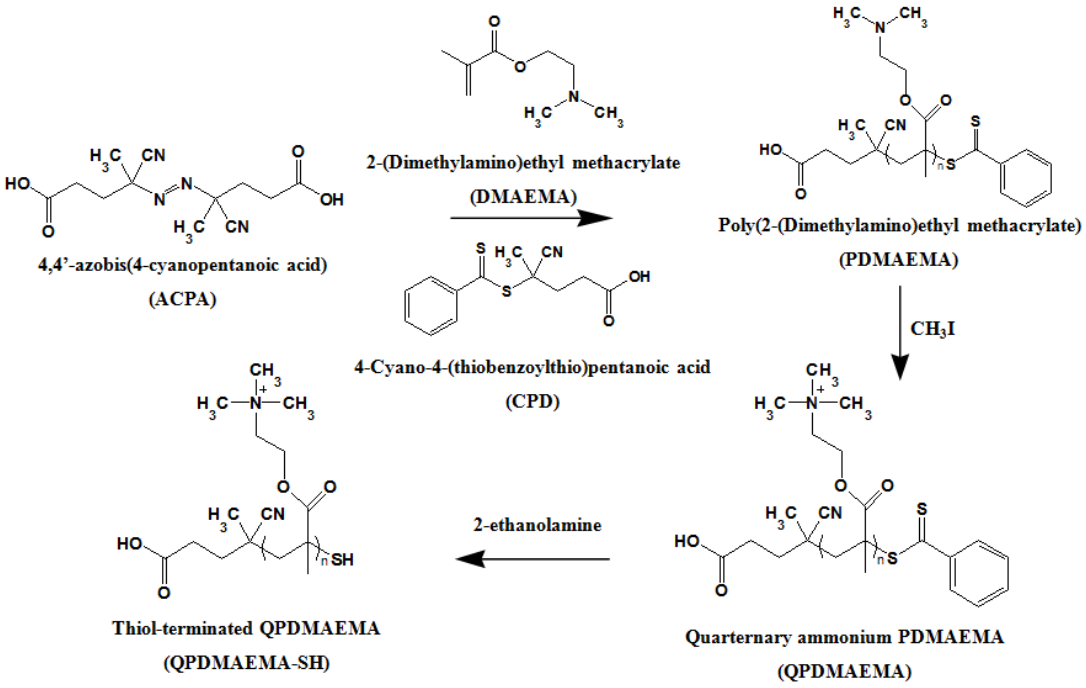


**Scheme 3.3** Synthesis of QPDMAEMA-SH by RAFT polymerization.

CPD (20.5 mg, $7.35 \times 10^{-5}$ mol) and ACPA (3.4 mg, $1.23 \times 10^{-5}$ mol) were added to the DMAEMA (1 mL, $590.00 \times 10^{-5}$ mol) solution in THF (970 µL). The solution was degassed by purging with nitrogen gas for 30 min, and then heated at 70 °C for 6 h. After being cooled down in an ice bath, the reaction mixture was dialyzed against DI water at ambient temperature for 3 days, before the PDMAEMA was recovered by lyophilization. To obtain the QPDMAEMA, PDMAEMA (59.0 mg, $37.50 \times 10^{-5}$ mol) were dissolved in MeOH (10 mL). After that, NaOH (30 mg, $75.00 \times 10^{-5}$ mol), NaI (56.2 mg, $37.5 \times 10^{-5}$ mol) and $CH_3I$ (70 µl, $112.50 \times 10^{-5}$ mol) were added to the solution. The reaction mixture was stirred for 6 h at 40 °C. The same amount of $CH_3I$ was added and the mixture was stirred for another 18 h at the same temperature. The solution was then dialyzed against 1M NaCl solution and DI water at ambient temperature for 1 and 2 days, respectively, before the QPDMAEMA was recovered by lyophilization. To remove the terminal dithiobenzoate group, an aqueous solution of QPDMAEMA was treated with 2-ethanolamine (30 mol equivalent of QPDMAEMA) and a trace amount of TCEP (3-5 mg) at ambient temperature for 24

h. The solution was dialyzed against DI water at ambient temperature for 3 days. The QPDMAEMA-SH was then obtained after lyophilization.

### 3.3.4 Synthesis of Gold Nanoparticles (AuNPs)

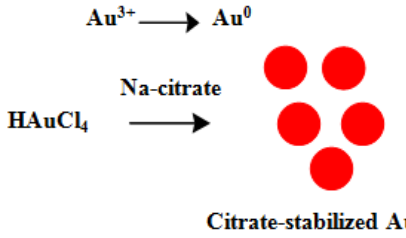


**Scheme 3.4** Synthesis of gold nanoparticles (AuNPs).

AuNPs was prepared according to a method modified from that of Hayat *et al.* [61]. All glasswares used for the synthesis of AuNPs, were washed with freshly prepared aqua regia solution ($HCl:HNO_3$ = 3:1, v/v) followed by extensive rinsing with distilled water prior to use. A boiling aqueous solution of $HAuCl_4$ (0.01% w/v, 50 mL) was added an aqueous solution of $Na_3$citrate (1% w/v, 1.75 mL). The mixture was heated for 30 min and cooled to room temperature. The color of the solution was changed from gray to red.

### 3.3.5 Preparation of AuNPs Stabilized by PNIPAM Monolayer (PNIPAM-AuNPs)

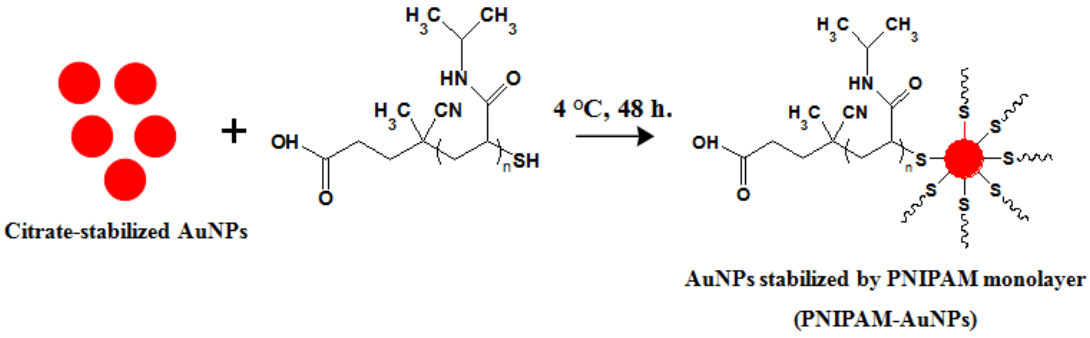


**Scheme 3.5** Preparation of PNIPAM-AuNPs.

PNIPAM-AuNPs were obtained by grafting to method modified from that of Zhu *et al.* [10]. According to Scheme 3.5, PNIPAM-SH ($0.2\times10^{-5}$ mol) was dissolved

in 10 mL of citrate-stabilized AuNPs solution which prepared from section 3.3.4. The solution was kept at 4 °C for 48 h. After that, excess PNIPAM-SH was removed from the PNIPAM-AuNPs by centrifugation at 14,000 rpm for 15 min. The precipitate was then dissolved in Milli-Q water.

### 3.3.6 Preparation of AuNPs Stabilized by Mixed Monolayer of PNIPAM and PAA (PAA/PNIPAM-AuNPs) or PNIPAM and QPDMAEMA (QPDMAEMA/PNIPAM-AuNPs)

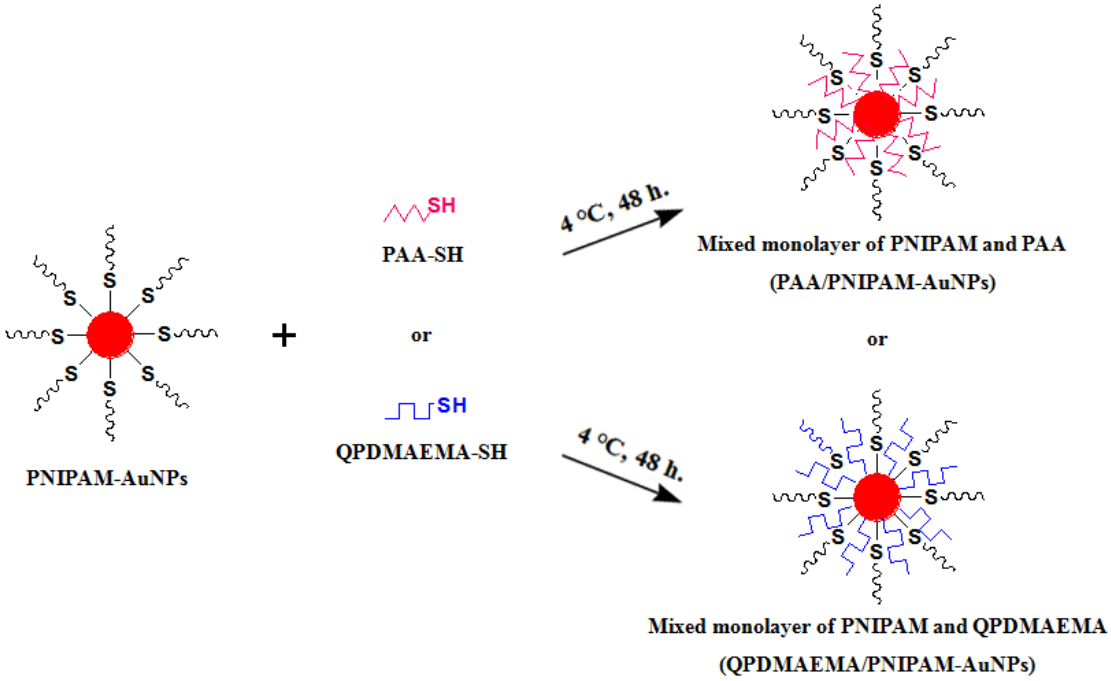


**Scheme 3.6** Preparation of PAA/PNIPAM-AuNPs and QPDMAEMA/PNIPAM-AuNPs.

PAA/PNIPAM-AuNPs were prepared by sequential grafting. Firstly, PNIPAM-SH was grafted on AuNPs by the same method described in section 3.3.5. Then, PAA ($0.2\times10^{-5}$ mol) was dissolved in 10 mL of PNIPAM-AuNPs solution resulting in PAA/PNIPAM-AuNPs formation. The solution was kept at 4 °C for 48 h. After that, excess PNIPAM-SH and PAA-SH were removed from the PAA/PNIPAM-AuNPs by centrifugation at 14,000 rpm for 15 min. The precipitate was then dissolved in Milli-Q water. The same method was used to prepare QPDMAEMA/PNIPAM-AuNPs except the PAA was replaced by QPDMAEMA.

## 3.4 Detection of Proteins

### 3.4.1 Determination of Fluorescence Quenching of Fluorophore by Polymer-stabilized AuNPs

In this part, the quenching efficiency of four fluorophores (G0 dendritic phenylene-ethynylene fluorophore) having different charges was studied with PNIPAM-AuNPs. The abbreviated names of the fluorophores are assigned according to the number and types of the functional groups on their peripheries in which $C^0$, $C^-$, $N^0$, and $N^+$ stand for carboxylate ester, carboxylic acid (or carboxylate anion in basic condition), amino, and quaternary ammonium groups, respectively. For examples, $C^02N^+$ possesses one carboxylate ester and two quaternary ammonium groups on its periphery [62].

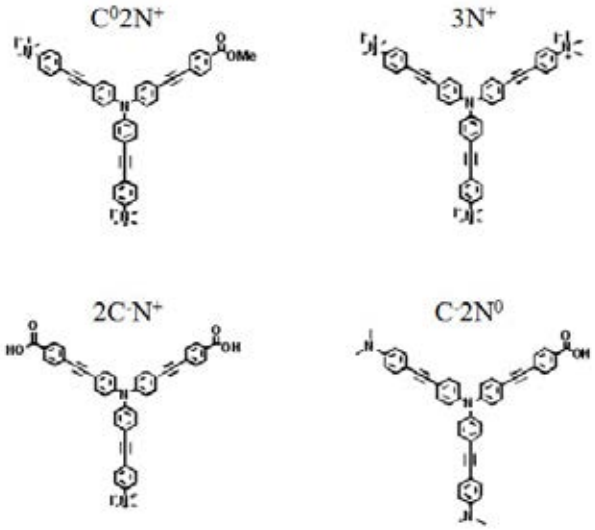


**Scheme 3.7** Chemical structures of G0 dendritic phenylene-ethynylene fluorophore.

In the first step, the fluorescent signal of fluorophore was determined by dissolving fluorophore ($1\times10^{-5}$ M, 100 µL) in 2,900 µL of PBS solution. After the solution was left for 30 min, it was analyzed by Luminescence Spectrometer. The second step was determined the quenching efficiency between fluorophore and PNIPAM-AuNPs. Fluorophore ($1\times10^{-5}$ M, 100 µl) was dissolved in 2,400 µl of PBS solution in a cuvette. After that, 500 µl of PNIPAM-AuNPs which prepared from section 3.3.5 were then added to the solution. To assure that the equilibrium was attained, the mixture was left for 30 min. Then, the mixture was analyzed by Luminescence Spectrometer.

### 3.4.2 Determination of Fluorescence Quenching of Fluorophore by Proteins

In this part, the fluorophore showing the least response with proteins were selected to be use for developing a sensor platform based on chemical nose approach. All of fluorophores from Scheme 3.7 were first tested with BSA. In the first step, fluorophore ($1\times10^{-5}$ M, 100 µL) was dissolved in 2,900 µL of PBS solution in a cuvette. After the solution was left for 30 min, the solution was analyzed by Luminescence Spectrometer. The second step, BSA (10 µL, 1 mg/mL) was then added to the mixture obtained from the first step. To assure that the equilibrium was attained, the mixture was analyzed by Luminescence Spectrometer after leaving for 30 min.

### 3.4.3 Determination of Protein Detection based on Fluorescence Quenching

In this part, the synthesized PNIPAM-AuNPs were put in an array-based sensing platform. Six types of proteins (BSA, Lys, Fib, Con A, Hgb, and TF) were analyzed by using four different types of PNIPAM-AuNPs having varied PNIPAM molecular weight and conformation (induced by thermal treatment) together with the G0 dendritic phenylene-ethynylene fluorophore having three positively charged $N(CH_3)_3^+$ groups per molecule ($3N^+$ fluorophore). There are four different types of PNIPAM-AuNPs were used fot this investigation. Two types were obtained from the AuNPs stabilized by 4 kDa of PNIPAM-SH (4k PNIPAM-AuNPs). The first type is 4k PNIPAM-AuNPs at 25 °C (NP1) which was obtained directly from section 3.3.5. The second type is 4k PNIPAM-AuNPs at 40 °C (NP2) which was obtained by heating 4k PNIPAM-AuNPs for 15 min and then leaving for 30 min to reach equilibrium. Another two types were obtained from AuNPs stabilized by 8 kDa of PNIPAM-SH (8k PNIPAM-AuNPs). The third type is 8k PNIPAM-AuNPs at 25 °C (NP3) and the forth type is 8k PNIPAM-AuNPs at 40 °C (NP4).

The detection of proteins was done as follows. In the first step, 500 µL of NP1 were dissolved in 2,400 µL of PBS. After that, $3N^+$ fluorophore ($1\times10^{-5}$ M, 100 µL) was then added and analyzed by Luminescence Spectrometer after equilibrium was reached for 30 min. The second step, BSA (10 µL, 1mg/mL) was added to the previous mixture and analyzed by Luminescence Spectrometer again after equilibrium

was reached for 30 min. BSA was subjected to the same analysis using NP2, NP3, and NP4. To generate an array-based sensing platform, other type of proteins was also detected with NP1, NP2, NP3, and NP4.

# CHAPTER IV
# RESULTS AND DISCUSSION

The aim of this work was to prepare a biosensor based on fluorescent quenching of fluorophore by AuNPs for proteins detection. This chapter is divided into three parts. The first part concentrated on the preparation and characterization of polymer-stabilized AuNPs by grafting-to technique. The second part is an attempt to prepare of PNIPAM-stabilized AuNPs by grafting-from technique. And the last part, the polymer-stabilized AuNPs were studied for protein detection.

## 4.1 Preparation and Characterization of Polymer-stabilized AuNPs by Grafting-to Technique

### 4.1.1 Synthesis and Characterization of Thiol-terminated Polymers

It is known that, polymers prepared by RAFT polymerization can be controlled by using a chain transfer agent. Besides, the dithioester group at the polymer chain end can be converted to a thiol group that is readily available for grafting onto the gold surface [63].

**Figure 4.1** shows the $^{1}$H-NMR spectra of the synthesized PNIPAM in comparison with NIPAM monomer. The strongest signal at 1 ppm can be assigned to the methyl protons of the side chain. The signals at 1.3, 1.8, and 3.7 ppm can be assigned to $H_{b,}$ $H_c$, and $H_d$ respectively. Percentage of conversion (% conversion) of NIPAM was calculated from the relative ratio between the peak integration of protons from the PNIPAM backbone ($H_c$) at 1.7-2.1 ppm and the sum of $H_c$ and $H_a$ at 5.9-6.1 ppm from NIPAM monomer, as shown in eqn. 4.1. The average molecular weight ($M_n$) of PNIPAM was calculated from the relative ratio between the peak integration of protons from the PNIPAM backbones ($H_c$) at 1.7-2.1 ppm and the peak integration of protons from the dithiobenzoate groups ($H_e$) at 7.3-7.9 ppm as shown in eqn. 4.2. From the data obtained, it was found that the % conversion and the average $M_n$ of PNIPAM were 41% and 4,053 g/mol and 42% and 7,015 g/mol for target DP of 70, respectively

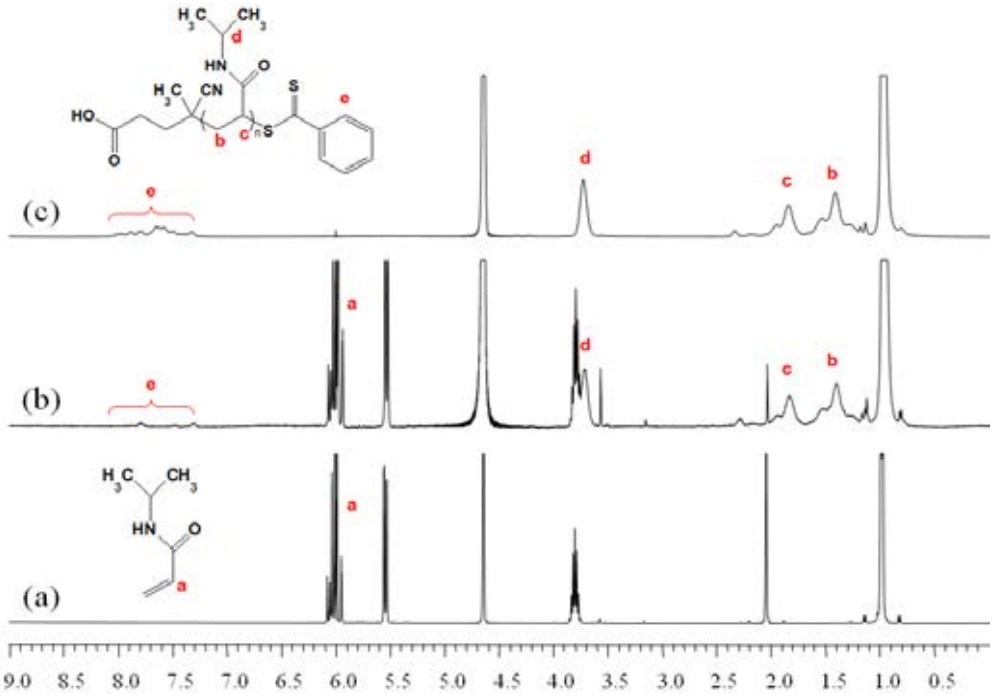


**Figure 4.1** $^{1}$H-NMR spectra of (a) NIPAM monomer, (b) non-purified PNIPAM, and (c) purified PNIPAM in $D_2O$.

$$\%\ \text{conversion} = \left\{ \frac{\text{intergral of the } H_c}{\text{intergral of the } H_c + \text{intergral of the } H_a} \right\} \times 100 \qquad (4.1)$$

$$\text{Average } M_n = \left\{ \frac{\text{intergral of the } H_c \times M_{n\,(\text{monomer})} \times \rho}{\left( \frac{\text{intergral of the } H_e}{5} \right)} \right\} + M_{n\,(\text{CPD})} \qquad (4.2)$$

**Figure 4.2** shows the $^{1}$H-NMR spectra of the synthesized PAA in comparison with AA monomer. Signals corresponding to $H_b$ and $H_c$ appeared at 1.7 and 2.3 ppm, respectively. The % conversion of AA was calculated from the relative ratio between the peak integration of protons from the PAA backbone ($H_c$) at 2.1-2.5 ppm and the sum of $H_c$ and $H_a$ at 5.9-6.0 ppm from AA monomer as shown in eqn. 4.1. The average $M_n$ of PAA was calculated from the relative ratio between the peak integration of $H_c$ and the peak integration of protons from the dithiobenzoate groups

($H_e$) at 7.3-7.9 ppm as shown in eqn 4.2. From the data obtained, it was found that the % conversion and average $M_n$ were 95% and 6,417 mol/g, respectively.

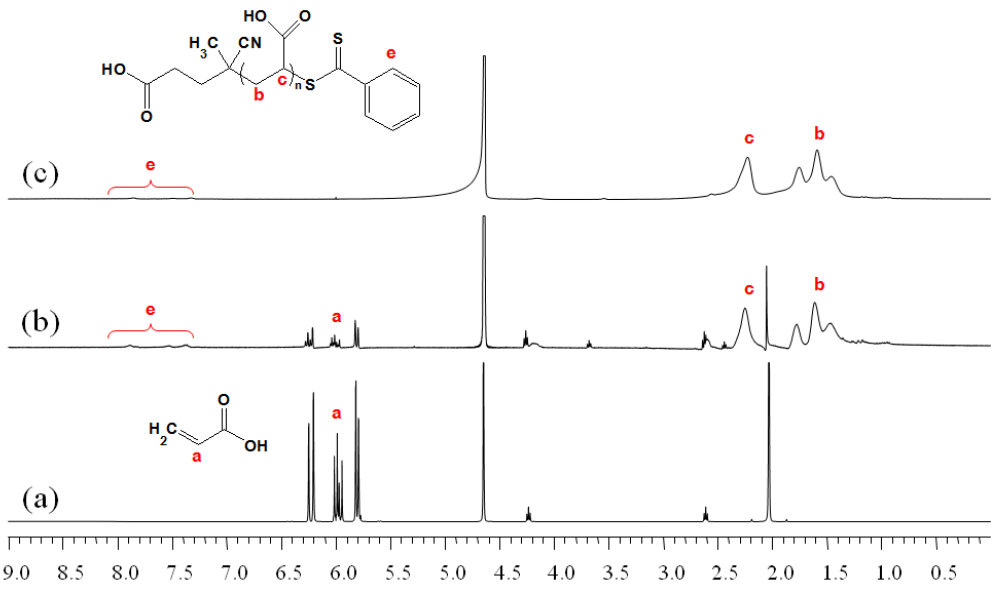


**Figure 4.2** $^1$H-NMR spectra of (a) AA monomer, (b) non-purified PAA, and (c) purified PAA**.**

**Figure 4.3** shows $^1$H-NMR spectra of synthesized PDMAEMA in comparison with PDMAEMA and DMAEMA monomer. Signals corresponding to $H_b$ and $H_c$ appeared at 0.8 and 1.8 ppm, respectively. The % conversion of DMAEMA was calculated from the relative ratio between the peak integration of protons from the PDMAEMA backbone ($H_c$) at 1.7-1.9 ppm and the sum of $H_c$ and $H_a$ at 5.9-6.0 ppm from DMAEMA monomer as shown in eqn. 4.1. The average $M_n$ of PDMAEMA was calculated from the relative ratio between the peak integration of $H_f$ at 3.7-4.3 ppm and the peak integration of protons from the dithiobenzoate groups ($H_g$) at 7.3-7.9 ppm as shown in eqn 4.3. Moreover, the downfield shift of the $H_d$ from 2.2-2.4 (6H) to 3.2-3.4 (9H), $H_e$ from 2.6-2.8 to 3.8-4.0, and $H_f$ from 4.0-4.3 to 4.4-4.7 ppm in **Figure 4.3d** of QPDMAEMA indicates that those protons became less electronegative as a consequence of quaternization. Furthermore, the peaks of $H_b$ and $H_c$ also shift to lower fields, however, the extent of this shift is moderate because these protons are far away from the reaction center [64]. In addition, it was found that the % conversion and average $M_n$ were 96% and 3,144 mol/g, respectively.

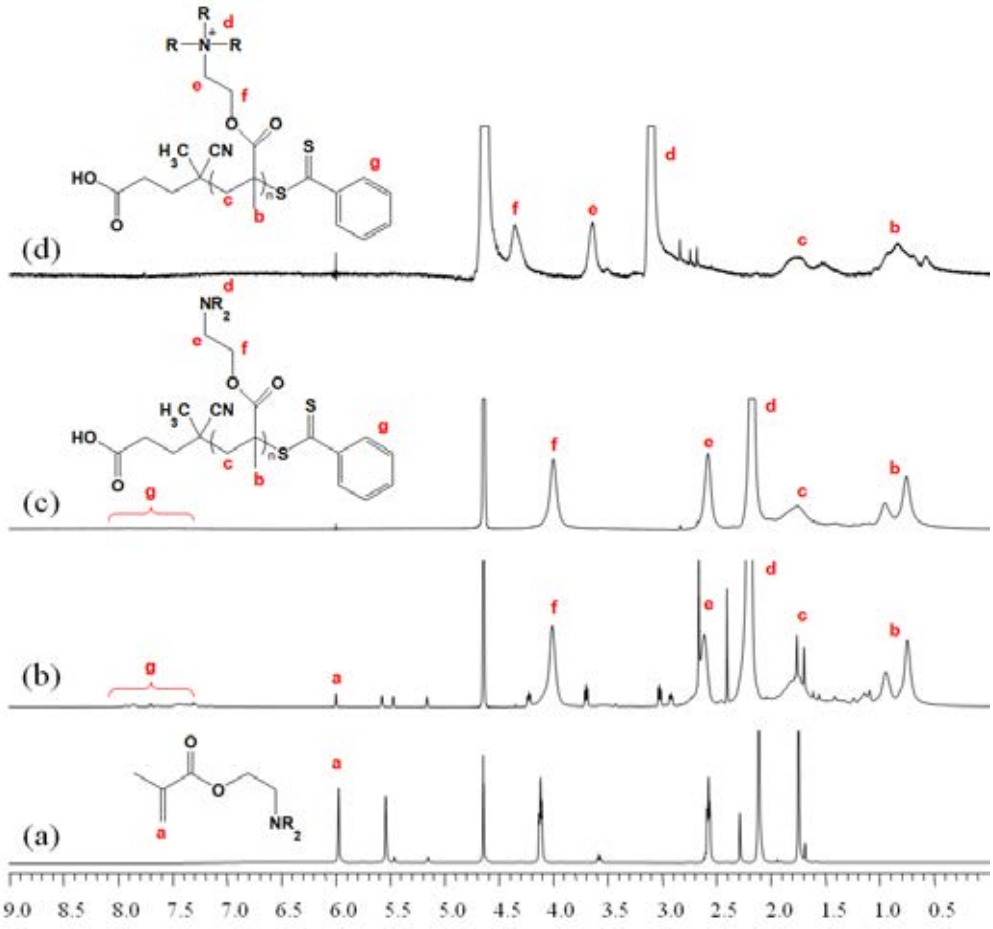


**Figure 4.3** $^{1}$H-NMR spectra of (a) DMAEMA monomer, (b) non-purified PDMAEMA, (c) purified PDMAEMA, and (d) purified QPDMAEMA**.**

$$\text{Average } M_n = \left\{ \frac{\left( \frac{\text{intergral of the } H_f}{2} \right) \times M_{n\,(\text{monomer})} \times \rho}{\left( \frac{\text{intergral of the } H_g}{5} \right)} \right\} + M_{n\,(\text{CPD})} \qquad (4.3)$$

The dithioester group at the polymer chain end can easily be cleaved by primary amine to yield the thiol group. Cleavage of the terminal dithiobenzoate group was confirmed by UV-vis absorption. In general, polymer prepared by the RAFT polymerization shows UV absorption around 300 nm due to the dithiobenzoate group at the chain end. **Figure 4.4** displays the UV-vis absorption spectra of PNIPAM before and after aminolysis by using 2-ethanolamine. PNIPAM spectrum exhibits the absorption maximum around 300 nm and that peak disappears when it was aminolized

(see PNIPAM-SH spectrum). In addition, the success of aminolysis was also confirmed by the appearance of PNIPAM which changed from pink-orange to white as a result from the cleavage of the terminal dithiobenzoate group. Similarly, after PAA and QPDMAEMA were aminolized, the absorption maximum around 300 nm also disappeared and the colors were changed from pink-orange to white.

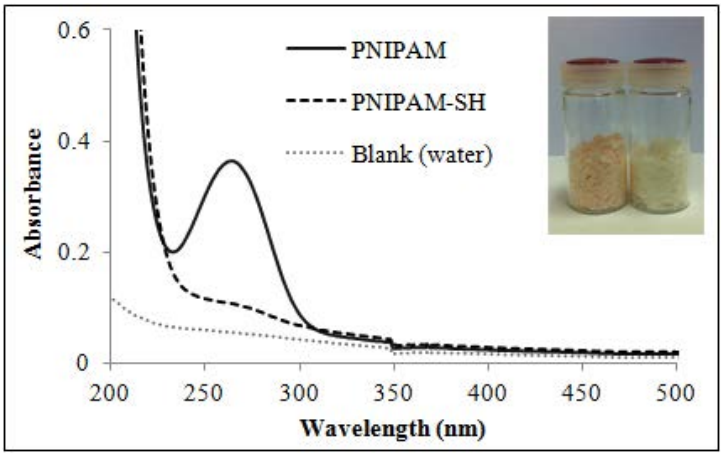


**Figure 4.4** UV-vis absorption spectra of PNIPAM and PNIPAM-SH in water**.**

Since the thiol-terminated polymers can easily be oxidized by oxygen, internal disulfide linkage may be formed and possibly yielded an overestimated molecular weight. To ensure that such incidence did not occur, the molecular weights of thiol-terminated polymers were also determined by GPC. According to the data shown in **Table 4.1**, it was found that the $M_n$ and PDI ($M_w/M_n$) values of the one before aminolysis and the one after aminolysis (thiol-terminated polymer) were closely resembled implying that the disulfide bond formation was absent [65]. The fact all PDI values are very close to one verifies that the molecular weight distribution is narrow and that the RAFT polymerization is living in character.

**Table 4.1** Molecular weight and polydispersity of polymer

| Polymer | Target | | [M]/[I]/[CTA] ($10^{-5}$ mol) | $M_n$[a] | PDI[a] | $M_n$[b] |
|---|---|---|---|---|---|---|
| | DP | $M_n$ | | | | |
| PNIPAM | 40 | 4,526 | 160.0/1/2.0 | 3,816 | 1.09 | 4,053 |
| | 70 | 7,921 | 314.5/1/2.5 | 8,552 | 1.13 | 7,015 |
| PNIPAM-SH | 40 | 4,526 | 160.0/1/2.0 | 4,180 | 1.11 | n/a |
| | 70 | 7,921 | 314.5/1/2.5 | 8,788 | 1.14 | n/a |
| PAA | 60 | 4,324 | 359.6/1/4.0 | n/a | n/a | 6,417 |
| PAA-SH | 60 | 4,324 | 359.6/1/4.0 | 4,360 | n/a | n/a |
| PDMAEMA | 60 | 9,433 | 481.6/1/6.0 | 5,899 | 1.13 | 3,144 |
| PDMAEMA-SH | 60 | 9,433 | 481.6/1/6.0 | 6,071 | 1.15 | n/a |

[a] determined by GPC analysis using THF as eluent
[b] calculated from $^1$H-NMR data

### 4.1.2 Preparation and Characterization of Polymer-stabilized AuNPs

It is known that, thiol-terminated polymers can directly bond to the surface of AuNPs through sulfur-gold interaction. So, thiol-terminated polymers which were synthesized from section 4.1.1 were grafted on AuNPs. Characteristic peaks of polymer-stabilized AuNPs were identified by FTIR anakysis. As compared with the FTIR spectrum of PNIPAM (**Figure 4.5a**), the FTIR spectrum of PNIPAM-AuNPs (**Figure 4.5b**) has a peak at 3,276 $cm^{-1}$ of N-H stretching from secondary amide, C-H deformation of isopropyl groups with a 1:1 intensity ratio at 1386 and 1367 $cm^{-1}$, indicated the success of PNIPAM-SH coating on the surface of AuNPs. As can be seen in **Figure 4.5c**, the FTIR spectrum of PAA has a peak at 1,726 $cm^{-1}$ assigned to the asymmetrical C=O stretch of the carboxylic acid group. However, this band is rather weak due to the interaction of the carboxyl groups with the AuNPs by formation of carboxylate groups [66]. We also found disappearance of C=O stretching of the carboxylic acid group at 1,716 $cm^{-1}$ and a new band around 1,654 $cm^{-1}$ assigned to the carboxylate groups in PAA-AuNPs (**Figure 4.5d**), indicated the PAA-SH can be grafted on AuNPs surface. The FTIR spectrum of QPDMAEMA is illustrated in **Figure 4.5f**. The appearance of C=O stretching from ester group at 1,728 $cm^{-1}$ and the appearance of C-N stretching peak at 1478 $cm^{-1}$ confirmed the success of the

QPDMAEMA synthesis. Characteristic peaks of QPDMAEMA found in the FTIR spectrum of QPDMAEMA-AuNPs, indicated the success of QPDMAEMA-SH attachment on the surface of AuNPs (**Figure 4.5g**).

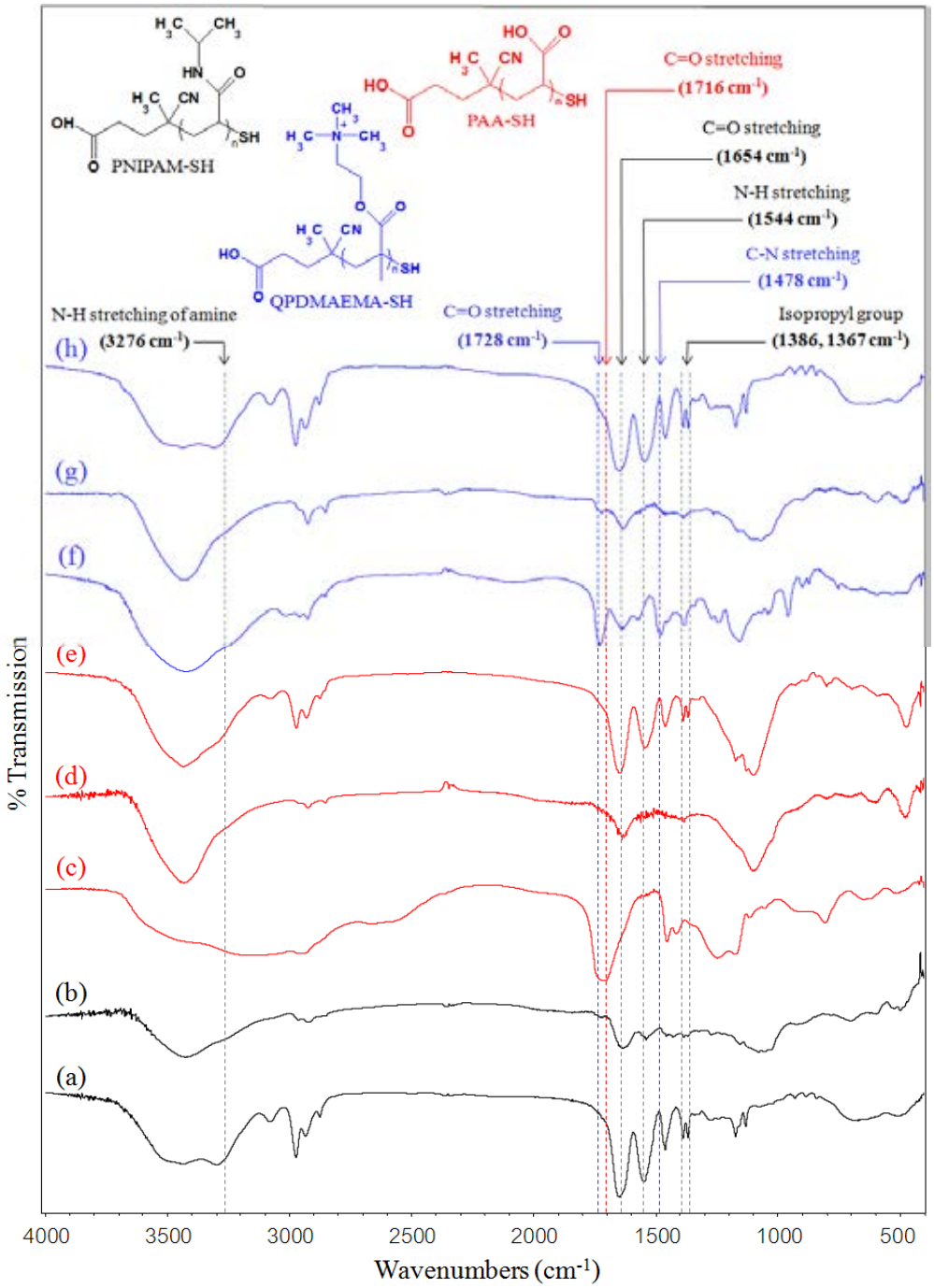


**Figure 4.5** FTIR spectra of (a) PNIPAM, (b) PNIPAM-AuNPs, (c) PAA, (d) PAA-AuNPs, (e) PAA/PNIPAM-AuNPs, (f) QPDMAEMA, (g) QPDMAEMA-AuNPs, and (h) QPDMAEMA/PNIPAM-AuNPs**.**

As observed in **Figure 4.5**, the FTIR spectra of PAA/PNIPAM-AuNPs (**Figure 4.5e**) and QPDMAEMA/PNIPAM-AuNPs (**Figure 4.5h**) were very similar that of the PNIPAM-AuNPs (**Figure 4.5d)**. This may be because the previously grafted PNIPAM-SH on AuNPs surface possessed high graft density. Therefore, it was difficult to insert PAA-SH or QPDMAEMA-SH on PNIPAM-AuNPs so that the signals of PAA and QPDMAEMA cannot be detected due to their small content.

The layer of PNIPAM shell surrounding the AuNPs can be visualized from AFM image shown in comparison with that of the uncoated AuNPs which was stabilized by citrate ions. In addition, we also studied the effects of molecular weights and concentrations of PNIPAM-SH grafted on AuNPs. As can be seen in **Figure 4.6**, the uncoated AuNPs were smaller than all of PNIPAM-AuNPs. For AuNPs surrounding with PNIPAM-SH, the particles size was increased with increasing molecular weight of PNIPAM. As shown in **Figure 4.6d-e**, the increasing of shell thickness was also obtained by increasing of PNIPAM-SH concentration. It was found that the proper concentration of PNIPAM-SH was 0.2 mM because it was the minimum concentration that still gave AuNPs with thermoresponsive property which can be observed by changing of AuNPs solution color after thermal treatment, the detail of which will be described in the following section.

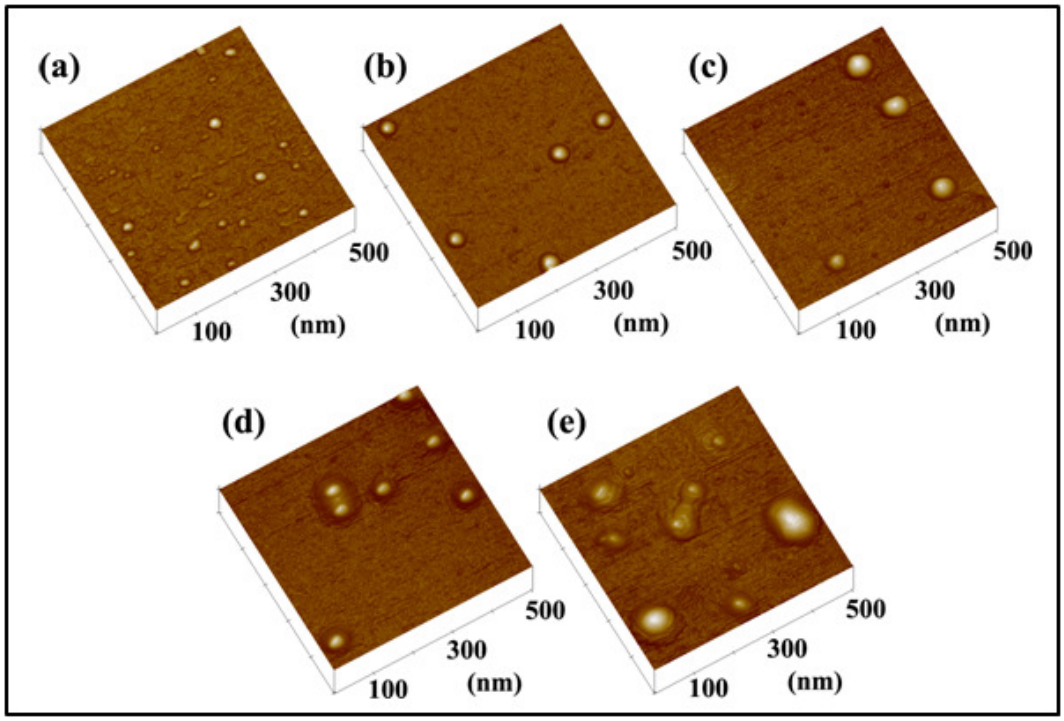


**Figure 4.6** AFM images of (a) uncoated AuNPs, (b) 4k PNIPAM-AuNPs (0.2 mM of PNIPAM-SH), (c) 8k PNIPAM-AuNPs (0.2 mM of PNIPAM-SH), (d) 4k PNIPAM-SH (0.5 mM of PNIPAM-SH), and (e) 8k PNIPAM-SH (0.5 mM of PNIPAM-SH)**.**

The grafting amount of two different molecular weights of PNIPAM-SH on flat gold surface was determined by using SPR analysis. From **Table 4.2**, 4k PNIPAM could be grafted with higher density and more consistent than 8k PNIPAM.

**Table 4.2** Amount of polymer chains grafted on the surface of flat SPR chip.

| Molecular weight of PNIPAM | 4k PNIPAM | | 8k PNIPAM | |
|---|---|---|---|---|
| Channel | 1 | 2 | 1 | 2 |
| Amount of polymer (ng/cm$^2$) | 824.25 | 824.25 | 229.42 | 373.83 |

We also attempted to estimate the graft density of two different molecular weights of PNIPAM-SH on flat gold surface by using AFM analysis. Nonetheless, the thickness of the grafted PNIPAM was so low that the analysis was not possible. The technique was not capable of distinguishing between the gold surface with and without the layer of polymer.

Surface plasmon band of AuNPs is known to be sensitive to the size of the particles and their surrounding environment. As shown in **Figure 4.7a**, highly dispersed AuNPs solutions exhibit a red color with an absorption band around 520 nm. The morphology and actual size was analyzed by TEM analysis (**Figure 4.7b**). Obviously, the particles were spherical in shape and showed uniform size distribution around 13 nm. To improve their stability via steric stabilization, the AuNPs were coated with PNIPAM. In principle, PNIPAM chains should be collapsed upon increasing temperature above its LCST of 32$^{o}$C which is a consequence of hydrogen bonding between water and PNIPAM being destroyed at elevated temperature. To determine the thermoresponsive behavior on AuNPs, PNIPAM-SH in PBS solution was subjected to temperature increase.

**Figure 4.7c** shows UV-vis absorption spectra of 4k PNIPAM-AuNPs at 25 and 40 °C in PBS solution. The absorption maximum of the plasmon band of 530 nm at 25 °C shifted to 551 nm when the temperature was increased to 40 °C. The color of the solution was changed from red to blue-purple without precipitation. The particles were still spherical in shape and consisted of 13 nm gold core and 1 nm PNIPAM shell, as can be seen in TEM image (**Figure 4.7d**). **Figure 4.7e** shows UV-vis absorption spectra of 8k PNIPAM-AuNPs at 25 and 40 °C in PBS solution. The absorption maximum of the plasmon band of 530 nm at 25 °C only slightly shifted to 541 nm after heating to 40 °C. This slightly red shift might be attributed to a high thickness of PNIPAM shell which prevented an aggregation of the AuNPs. This result was consistent with the color of the solution in that the solution was changed from red to pink-purple without precipitation. The morphology and actual size were also displayed in **Figure 4.7f**. The particles were spherical in shape with well defined core/shell nanostructures which is also consisted of a 13 nm gold core and 14-17 nm PNIPAM shell.

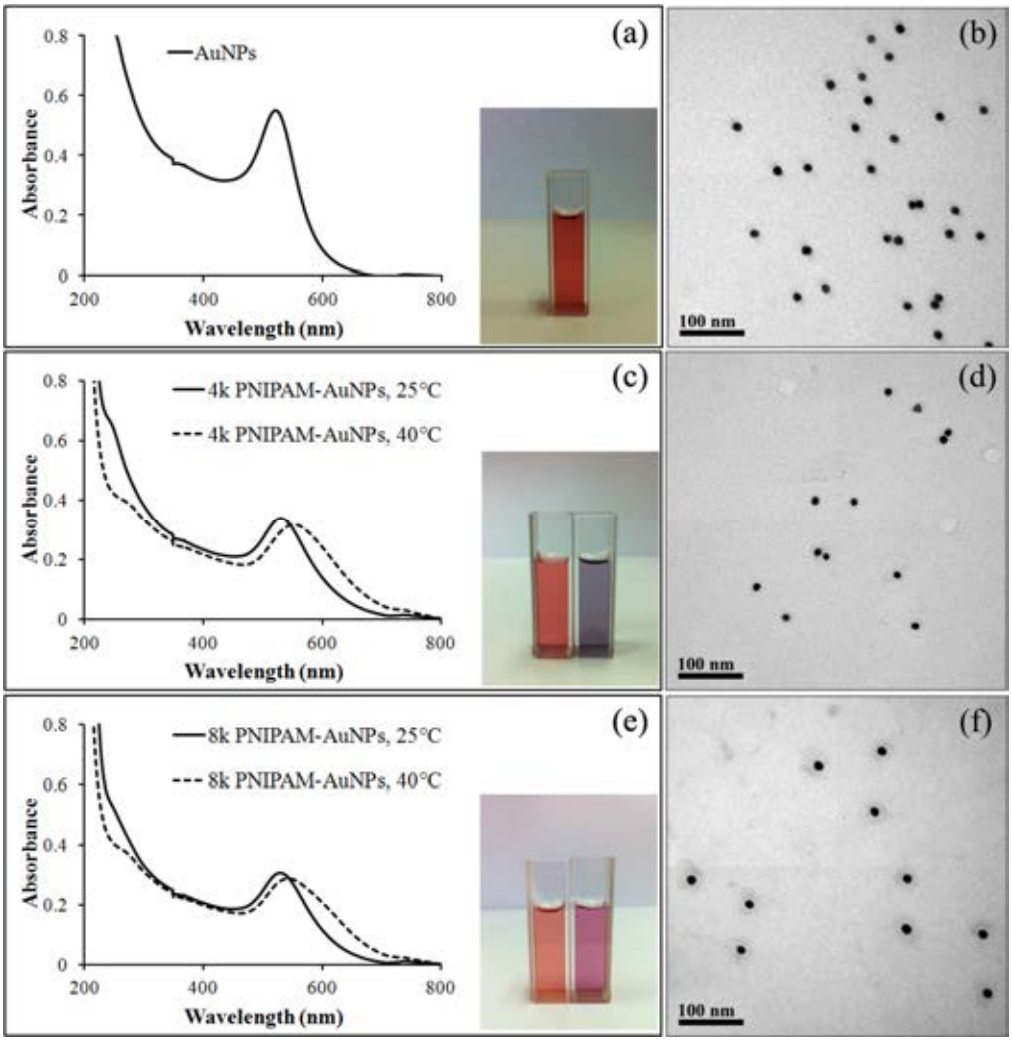


**Figure 4.7** UV-vis spectra and TEM images of polymer-stabilized AuNPs.

The particles size obtained from AFM and TEM analysis were measured by using Semafore program. The results are summarized in **Table 4.3**.

**Table 4.3** Paticle size obtained from AFM and TEM analysis.

| Particles | Size (nm) | |
|---|---|---|
| | AFM[a] | TEM[b] |
| AuNPs | 19.86 ± 5.9 | 13.98 ± 0.91 |
| 4k PNIPAM-AuNPs | 39.39 ± 1.49 | 15.36 ± 0.86 |
| 8k PNIPAM-AuNPs | 59.90 ± 4.51 | 42.08 ± 6.30 |

[a] measured from 10 particles of AuNPs by using Semafore program
[b] measured from 20 particles of AuNPs by using Semafore program

Furthermore, we aimed to study the effect of positive and negative charge of AuNPs on protein detection by additional grafting of PAA-SH and QPDMAEMA-SH on PNIPAM-AuNPs. To graft PAA-SH and QPDMAEMA-SH on the surface of PNIPAM-AuNPs, the molecular weight of PAA-SH and QPDMAEMA-SH should be smaller than PNIPAM-SH so that the insertion of PAA-SH or QPDMAEMA-SH on the space between PNIPAM chains were possible. So, AuNPs stabilized by high molecular weight of PNIPAM (8k PNIPAM-AuNPs) were selected for the preparation of PAA/PNIPAM-AuNPs and QPDMAEMA/PNIPAM-AuNPs.

**Figure 4.8** shows the UV-vis spectra of PAA/PNIPAM-AuNPs and QPDMAEMA/PNIPAM-AuNPs at 25 and 40 °C in PBS solution. It was found that these particles did not show the thermoresponsive behavior. The absorption maximum of the plasmon band of PAA/PNIPAM-AuNPs and QPDMAEMA/PNIPAM-AuNPs was not shifted with increasing temperature. It might be attributed to the decreasing of graft density of PNIPAM-SH due to PAA-SH or QPDMAEMA-SH replacement.

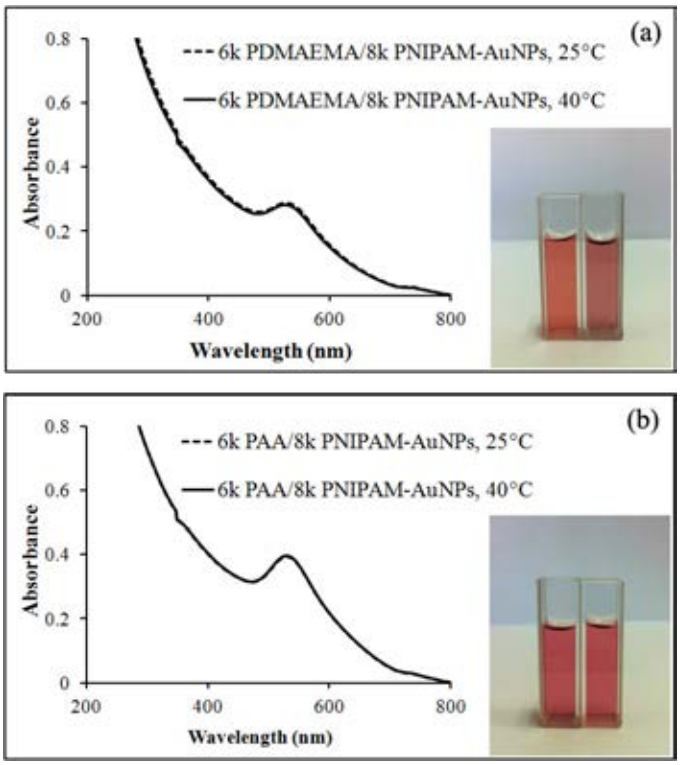


**Figure 4.8** UV-vis spectra of (a) PAA/PNIPAM-AuNPs and (b) QPDMAEMA/PNIPAM-AuNPs**.**

## 4.2 Attempt to Prepare of PNIPAM-stabilized AuNPs by Grafting-from Technique

We also attempted to prepare PNIPAM-AuNPs via grafting from technique. An initiator was first immobilized on the surface of hydroxyl group functionalized AuNPs, previously prepared by $HAuCl_4$ reduction in the presence of hydroxyl-terminated alkanethiol. Noticeably, the thiol-terminated initiator can be linked onto gold surface via the direct gold-sulfur covalent bond. Then, the initiator-modified AuNPs were subjected to polymerization of NIPAM. In principle, the polymer chains should grow from a monolayer of the initiator. We expect that polymer brushes can be obtained with relatively high grafted density.

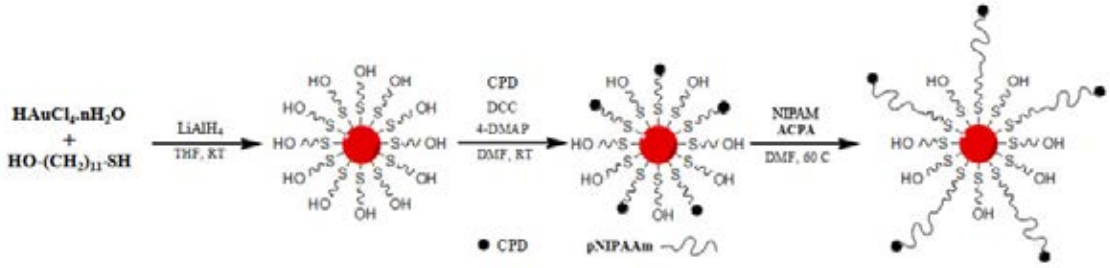


**Scheme 4.1** Reaction steps for the preparation of PNIPAM- stabilized AuNPs by grafting from technique**.**

For the experiment, PNIPAM-AuNPs was prepared by a method modified from that reported Raula *et al.* [11]. As shown in **Scheme 4.1**, the preparation was divided into three steps. The first step was to prepare hydroxyl group functionalized AuNPs (MUD-AuNPs). MUD stands for mercaptoundecanol ($OH(CH_2)_{11}SH$). $HAuCl_4$ (3.54 mg, $0.93x10^{-5}$ mol) was dissolved in THF (10 mL) and stirred for 15 min. MUD ($0.90\ x10^{-5}$ mol) was gradually added to the mixture while stirring. Then the mixture was stirred for 30 min until the color was changed from brown to orange (**Figure 4.9a**). After that, the formation of AuNPs by $LiAlH_4$ reduction was conducted at room temperature. $LiAlH_4$ as a reducing agent was slowly added to the mixture with vigorous stirring. After adding strong reductant, the solution was changed to a black suspension and the temperature of the mixture was slightly increased (**Figure 4.9b**). The solution was further stirred until the temperature of the mixture decreased back to room temperature. Purification of the AuNPs was conducted by centrifugation (14,000 rpm) in an ethanol/THF mixture.

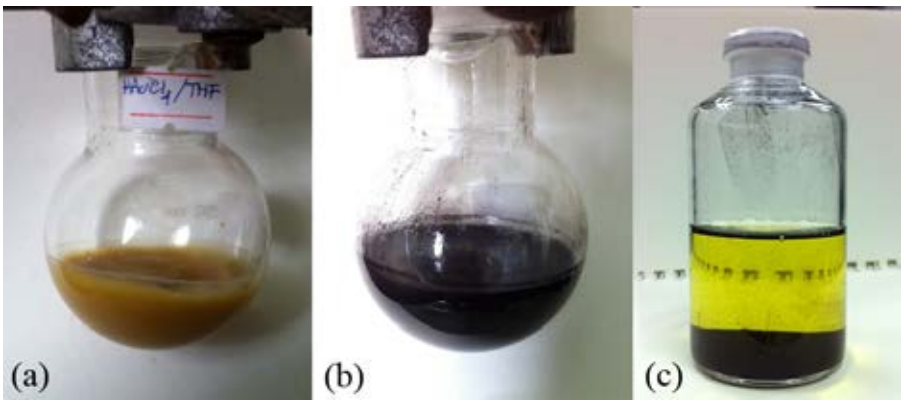


**Figure 4.9** Appearance of MUD-AuNPs.

The second step was the preparation of initiator-immobilized AuNPs, CPD-AuNPs via coupling reaction between hydroxyl group on AuNPs and carboxyl group of CPD using DCC as a coupling agent. MUD-AuNPs (155 mg) prepared from the first step, DCC (0.12 mmol) and 4-DMAP (0.01 mmol) were dissolved in 9 mL of DMF and flushed with dry nitrogen for 15 min. CPD (0.04 mmol) dissolved in 1 mL of DMF was added dropwise to the mixture with stirring at room temperature. After that, the temperature of the reaction mixture was heated to 30 °C, and kept at this temperature for 48 h. The purification of the product was accomplished by dialysis in DI water at ambient temperature for 3 days. The CPD-AuNPs was then obtained after lyophilization. PNIPAM-AuNPs was prepared in the third step. CPD-AuNPs (70 mg), ACPA (0.0004 mmol), and NIPAM (2.1 mmol) were dissolved in 1.5 mL of DMF. Oxygen in the reaction was removed by purging with nitrogen gas for 30 min. Then, the mixture was placed in an oil bath at 70 °C for 48 h. After the polymerization, the PNIPAM-AuNPs was isolated by the precipitation in diethyl ether. Then, the precipitate was collected and washed with THF by centrifugation (5000 rpm).

After attempt to prepare PNIPAM-AuNPs via grafting-from method, we found that the obtained PNIPAM-AuNPs were extremely aggregated. It may be because the stabilizer (MUD) is not enough to stabilize AuNPs resulting in AuNPs aggregation. Therefore, we tried to adjust the aspect ratio between $HAuCl_4$ and MUD and found that size of PNIPAM-AuNPs was decreased with increasing of MUD as shown in **Figure 4.10**. However, they were still aggregated. So, we have desired not to investigate further the preparation of PNIPAM-AuNPs by grafting-from technique.

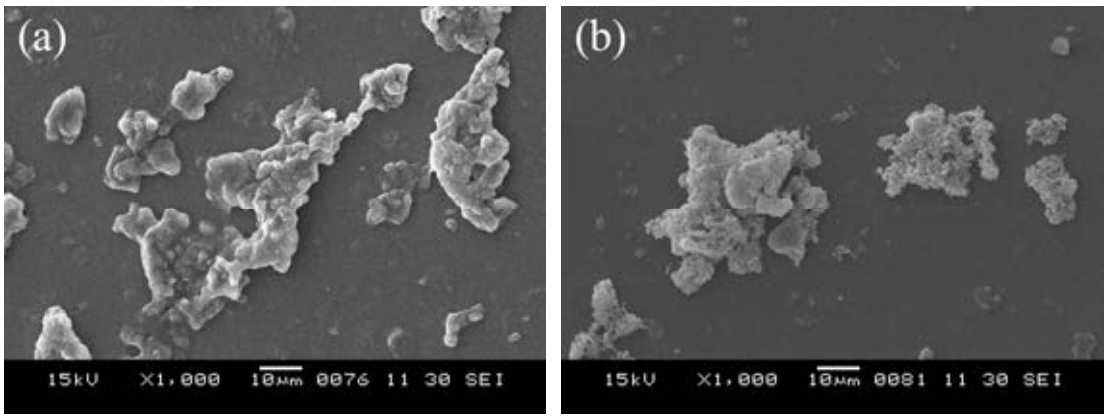


**Figure 4.10** SEM image of PNIPAM-AuNPs synthesized by grafting-from method using different mole ratio of (a) Au:MUD = 1:1 and (b) Au:MUD = 1:5.

## 4.3 Detection of Proteins

To put the synthesized PNIPAM-AuNPs in an array-based sensing platform, a preliminary protein detection was performed using 4 different types of PNIPAM-AuNPs having varied PNIPAM molecular weight and conformation (induced by thermal treatment) together with fluorophore. The results of fluorescent response are described in the following sections.

### 4.3.1 Determination of Fluorescence Quenching of Fluoreophore by Polymer-stabilized AuNPs

The quenching efficiency of four fluorophores (G0 dendritic phenylene-ethynylene fluorophore) having different charges (structure shown in **Scheme 3.1**, Chapter 3) were studied with 4k PNIPAM-AuNPs at 25 °C. As presented in **Figure 4.11**, the $C^-2N^0$ and $2C^-N^+$ fluorophores were slightly quenched, while the $3N^+$ and $C^02N^+$ fluorophores were largely quenched by using 4k PNIPAM-AuNPs as quencher. The $C^-2N^0$ fluorophore has one carboxylic acid and two amino groups resulting in -1 electronic charge.The $2C^-N^+$ fluorophore has two carboxylic acid and one quaternary ammonium group resulting -1 electronic charge. Therefore, there should by the repulsive force between PNIPAM-AuNPs which have lone paired electrons of nitrogen and oxygen in repeating unit and $C^-2N^0$ or $2C^-N^+$ fluorophores. That is why the quenching was ineffective. On the other hand, $3N^+$ fluorophore has three quaternary ammonium groups resulting in +3 electronic charge. $C^02N^+$ fluorophore have one carboxylate ester and two quaternary ammonium groups

resulting in +2 electronic charge. Therefore, there should be electrostatic interactions between PNIPAM-AuNPs and $3N^+$ or $C^02N^+$ fluorophoresthat made the quenching more effective. For this reason, only$3N^+$ and $C^02N+$ fluorophores were subjected for further investigation. The percentages of quenching efficiency of four fluorophores are shown in **Figure 4.12**

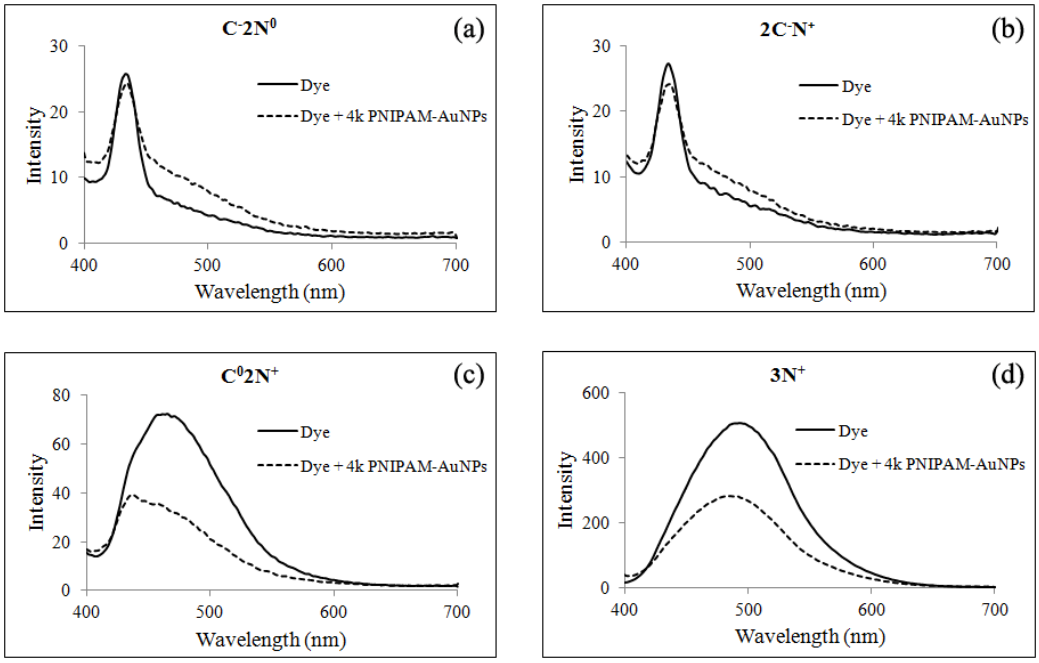


**Figure 4.11** Absorption spectra demonstrating quenching behavior of four G0 dendritic phenylene-ethynylene fluorophores: (a) $C^-2N^0$, (b) $2C^-N^+$ (c) $3N^+$, and (d) $C^02N^+$ by using 4k PNIPAM-AuNPs as a quencher.

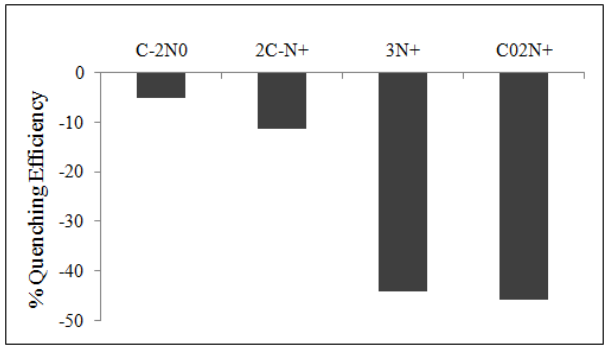


**Figure 4.12** Percentage of quenching efficiency of four G0 dendritic phenylene-ethynylene fluorophores having different charge by using 4k PNIPAM-AuNPs as a quencher.

### 4.3.2 Determination of Fluorescence Quenching of Fluorophore by Proteins

To assure that the change in fluorescence response was initiated from quenching by the AuNPs, the interactions between the fluorophore and protein were investigated. The fluorophore having the least response with proteins should be the most appropriate one to be used for the development of protein sensor based on fluorescence quenching. As can be seen in **Figure 4.13**, it was found that the absorption intensity of $3N^+$ fluorophore was minimally affected by BSA. Therefore, $3N^+$ fluorophore was selected for further investigation. The percentages of the change in absorption intensity of four fluorophores upon BSA addition are outlined in **Figure 4.14**.

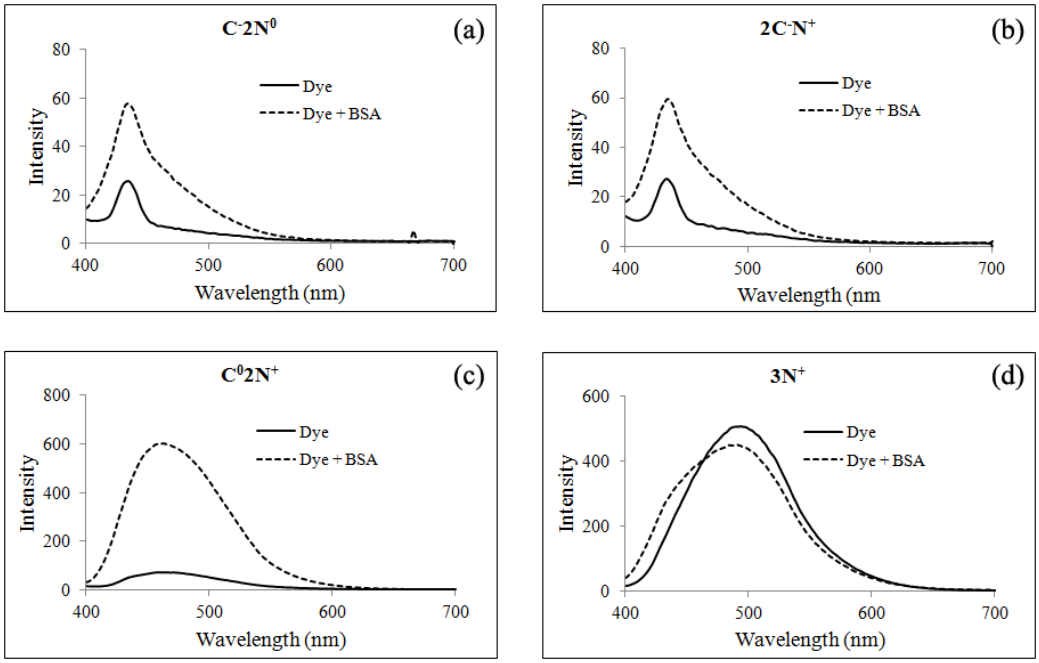


**Figure 4.13** Absorption spectra demonstrating the change in absorption intensity of four G0 dendritic phenylene-ethynylene fluorophores: (a) $C^-2N^0$, (b) $2C^-N^+$ (c) $3N^+$, and (d) $C^02N^+$ upon BSA addition.

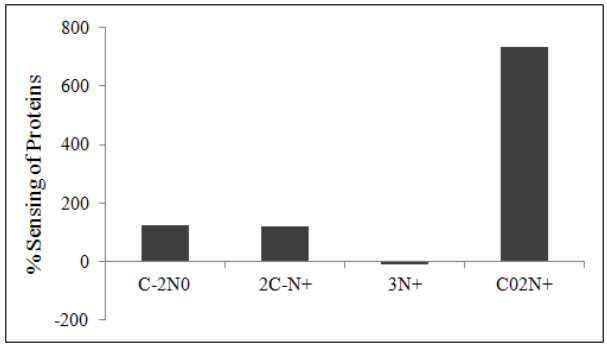


**Figure 4.14** Percentage of the change in absorption intensity of four G0 dendritic phenylene-ethynylene fluorophores having different charge upon BSA addition.

To confirm that the $3N^+$ fluorophore was a proper dye, it was also tested with six different types of protein having different pI and MW (**Table 4.4**). It was found that all types of proteins could not enhance the intensity of fluorescent signal of $3N^+$ fluorophore (**Figure 4.15**).

**Table 4.4** Properties of each protein used as a biomarker

| Proteins | BSA | Lys | Fib | Con A | Hgb | TF |
|---|---|---|---|---|---|---|
| Mw (kDa) | 67 | 14 | 270 | 27 | 17 | 76 |
| pI | 4.6 | 11.0 | 5.5 | 6.5 | 6.8 | 5.8 |

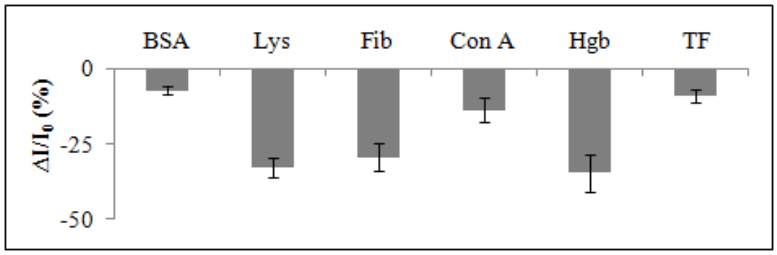


**Figure 4.15** Percentage of the change in emission intensity of $3N^+$ fluorophore when tested with six proteins

Moreover, six different types of AuNPs: 4k PNIPAM-AuNPs, 25°C (NP1), 4k PNIPAM-AuNPs, 40°C (NP2), 8k PNIPAM-AuNPs, 25°C (NP3), 8k PNIPAM-AuNPs, 40°C (NP4), 6k PAA/8k PNIPAM-AuNPs, 25°C (NP5), and 6k QPDMAEMA/8k PNIPAM-AuNPs, 25°C (NP6) were subjected to investigation on their quenching efficiency on $3N^+$ fluorophore.

To study the effect of polymer conformation grafted on AuNPs surface on the quenching efficiency, NP1 and NP2 were compared. **Figure 4.16** shows that the quenching efficiency of NP2 was higher than NP1. This may be because PNIPAM on NP2 were heated to 40 °C (upper LCST). The polymer conformation changed from stretch to coil structure resulting in the decreasing of distance between AuNPs and fluorophore and so the enhanced degree of quenching. To study the effect of polymer molecular weight, NP1 and NP3 were compared. It was found that the quenching efficiency of NP1 was greater than NP3. This may be explained as a result of the PNIPAM layer on the NP1 being thinner than that on the NP3. The closer distance between the AuNPs surface and fluorophore in the case of NP1 when compared to that of the NP3 thus promotes the quenching process. In the case of charged AuNPs (NP5 and NP6), it was found that NP5 possessed the highest quenching efficiency when compared with other AuNPs. This may be due to the negative charges of the PAA grafted on the negatively charged NP5 can easily attract the positively charged $3N^+$ fluorophore via electrostatic interactions. The close proximity between the fluorophore and the AuNPs, therefore, let to the highly efficient quenching. The result turned out in the opposite direction in the case of positively charged NP6 of which quenching efficiency was the lowest among all AuNPs tested. The lowest quenching efficiency can be attributed to the repulsive forces between the positive charges of QPDMAEMA grafted on the NP6 and the positively charged $3N^+$ fluorophore. In addition, the variation in quenching efficiency of NP5 NP6 which are different from that of the NP3 can possibly be used as qualitative evidence of PAA-SH and QPDMAEMA-SH grafting on the PNIPAM-AuNPs.

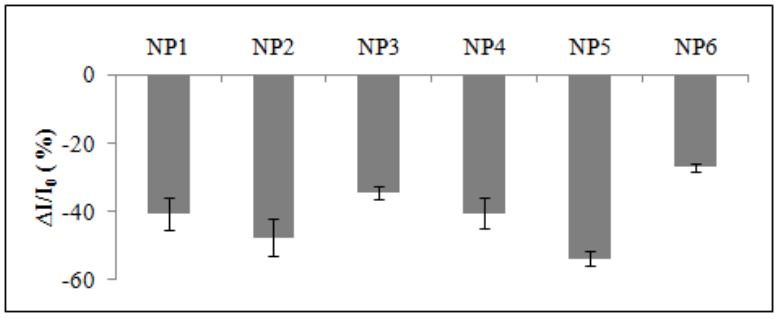


**Figure 4.16** The quenching efficiency of six types of AuNPs with $3N^+$ fluorophores.

### 4.3.3 Determination of Protein Detection based on Fluorescence Quenching

In this part, six types of proteins were analyzed by using NP1-NP4 with the $3N^+$ fluorophore. **Figure 4.17a** shows absorption spectra demonstrating quenching behavior of $3N^+$ fluorophore in the presence of BSA and NP1. As can be seen in the spectrum of $3N^+$ fluorophore (solid line), the highest intensity of fluorescent signal appeared around 230 unit. When NP1 was added to the $3N^+$ fluorophore solution, the intensity of fluorescent signal decreased to 80 unit due to energy transfer from fluorophore to AuNPs. After an addition of BSA to the mixed solution of NP1 and $3N^+$ fluorophore, the intensity of fluorescent signal was clearly increased again. At pH 7.4, the $3N^+$ fluorophore should be positively charged while the BSA should be negatively charged. As a result, the release of $3N^+$ fluorophore from AuNPs surface can be induced by electrostatic interactions between the fluorophore and BSA so that the $3N^+$ fluorophore can emit the fluorescent signal again. This is only possible when the electrostatic interactions between the fluorophore and BSA are stronger than the charge-dipole interactions between the fluorophore and the PNIPAM layer on the AuNPs surface of NP1. **Figure 4.17b** illustrates the percentage of the change in fluorescent response of $3N^+$ fluorophore in the presence of NP1 and six proteins. Such change can be determined from a difference in maximum intensity between before and after protein addition. These preliminary results indicated that it is possibile to use this sensing platform for identifying each type of proteins based on the variation in fluorescent response which depends on the protein type.

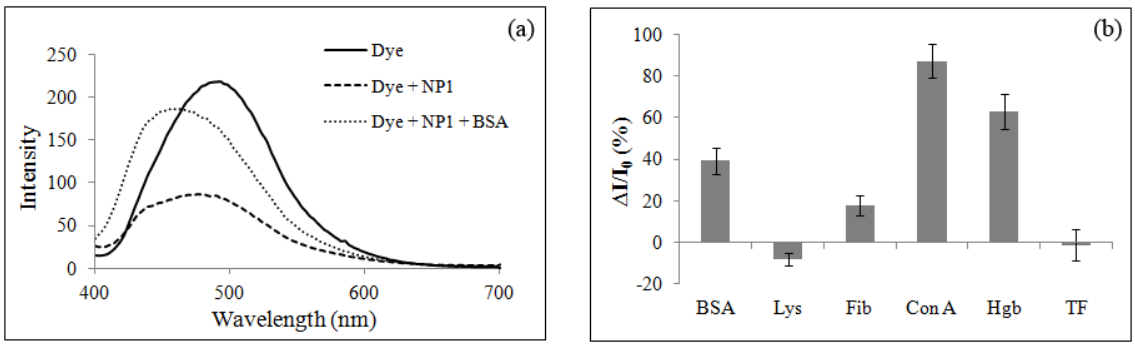


**Figure 4.17** Fluorescence emission spectra demonstrating quenching behavior of $3N^+$ fluorophore in the presence of NP1 and BSA (a) and percentage of the change in emission intensity of $3N^+$ fluorophore when tested with six proteins using NP1(b).

Moreover, NP2, NP3 and NP4 were also tested for protein detection to generate an array based sensing platform. The obtained results are illustrated in **Figure 4.18**. Each type of PNIPAM-AuNPs exhibited a different response with each type of proteins. The fluorescent responses of six proteins when using NP1 were larger than other three types of PNIPAM-AuNPs. Unlike NP1, NP2 with its thinner PNIPAM layer may provide stronger interactions with the fluorophore due to the closer distance between the gold core and the fluorophore which can be explained from its greater quenching efficiency when compared with NP1 (See **Figure 4.16**). For this reason, it might be difficult for the fluorophore to be released from NP2 surface upon the protein addition. The collapsed PNIPAM layer in the case of NP2 may give additional difficulty for the fluorophore trapped inside the polymer to be released out. That is why the signal responses were not high. In the case of NP3, of which PNIPAM layer was thicker than that of NP1, the change in fluorescence response was proportionally smaller. We explained this as a consequence of the quenching being initially low even before the protein addition due to the long distance between the gold core and the fluorophore (See **Figure 4.16**). After the addition of protein, the fluorescence signal was not much affected and therefore gave the relatively low response. Despite the facts that the PNIPAM layer of NP4 was thinner than that of the NP3 and its initial quenching efficiency was as high as that of NP1, overall signal responses of NP4 were relatively small and followed the same trend that observed in the case of NP3. We suspect that the same explanation previously used for NP2 based on the difficulty in releasing the entrapped fluorophore from the condensed layer of PNIPAM can be applied here.

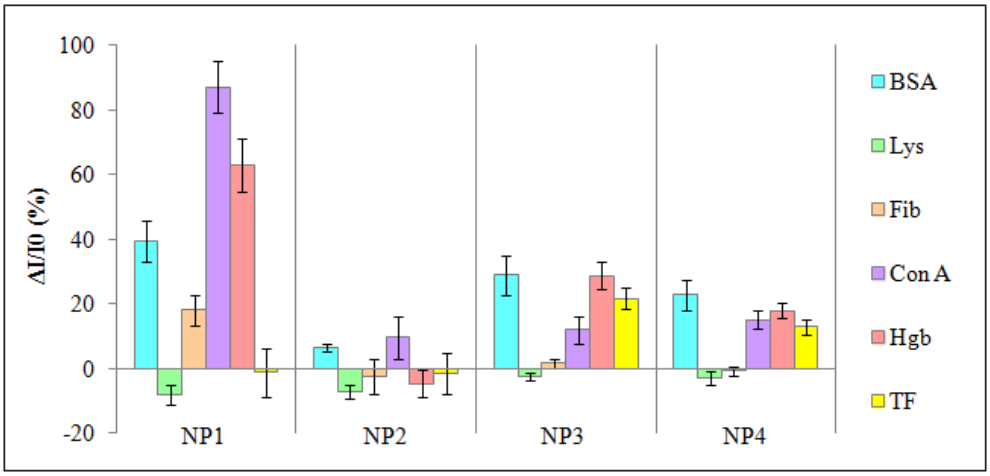


**Figure 4.18** Histogram plot of fluorescent response ($\Delta I/I_0$) patterns of $3N^+$ fluorophore in the presence of six proteins in PBS for each type PNIPAM-AuNPs (responses are averages of six measurements and error bars are standard deviations).

For AuNPs having negative charges, 6k PAA/8k PNIPAM-AuNPs (NP5), it was found that the fluorescent signals cannot be recovered after protein addition (BSA and Lys) implying that the electrostatic interactions between NP5 and the $3N^+$ fluorophore were so strong that the fluorophore cannot be released (**Figure 4.19**). In contrast, the signal of $3N^+$ fluorophore was slightly quenched by the positively charged 6k QPDMAEMA/8k PNIPAM-AuNPs (NP6) due to the repulsive force of the same charges. Nevertheless, the fluorescence signals were not much affected by the addition of BSA and Lys. For this reason, NP5 and NP6 were considered as not suitable platforms for protein detection based on fluorescence quenching mode.

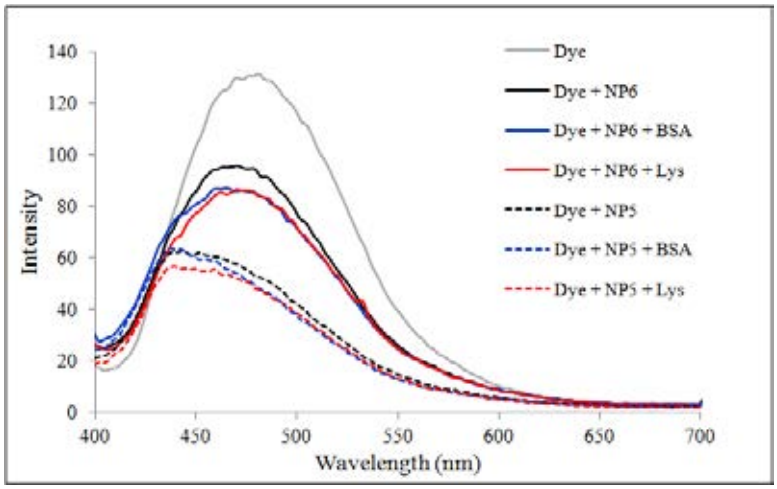


**Figure 4.19** Absorption spectra demonstrating quenching behavior of $3N^+$ fluorophore in the presence of NP5 and NP6 before and after protein (BSA.and Lys) addition.

To demonstrate the protein detection profile of the developed sensing array based on four types of PNIPAM-AuNPs, the histogram in **Figure 4.18** was replotted for each PNIPAM-AuNPs and shown in **Figure 4.20**. It is obvious that the responsive pattern of each AuNPs were varied with the type of protein because of the difference in charge and molecular weight of protein, the information of which is summarized in **Table 4.5**.

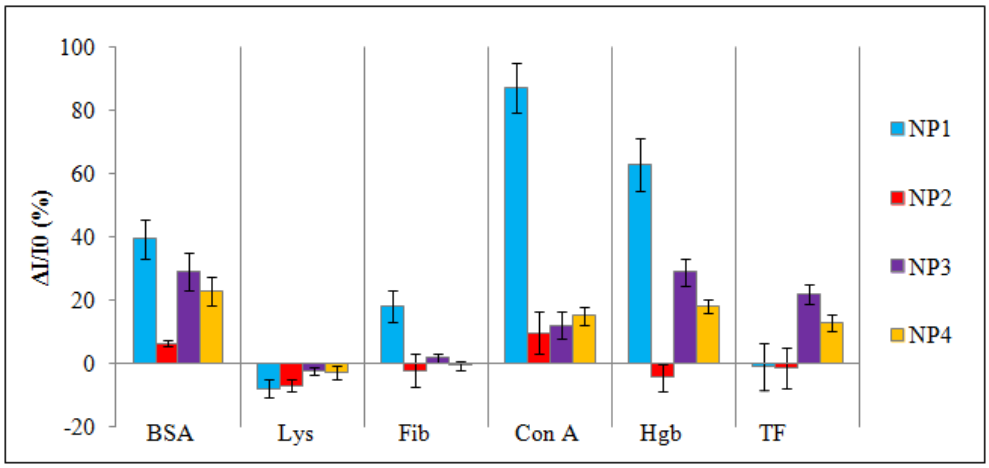


**Figure 4.20** Histogram plot of fluorescent response ($\Delta I/I_0$) patterns of $3N^+$ fluorophore in the presence of PNIPAM-AuNPs for each type of proteins in PBS (responses are averages of six measurements and error bars are standard deviations).

It is known that at pH 7.4, the $3N^+$ fluorophore bound on the AuNPs surface via charge-dipole interactions. Therefore, when the negatively charged proteins (BSA, Fib, Con A, Hgb, and TF) were added, the release of $3N^+$ fluorophore from the AuNPs surface driven by the electrostatic interactions between negatively charged proteins in solution and $3N^+$ fluorophore can take place so that the quenched fluorescent signal can be recovered. Although being negatively charged proteins, Fib and TF did not provide responses against some types of AuNPs. These might be caused by their high molecular weight being obstacle for effective binding with $3N^+$ fluorophore and thus hampering the fluorescence signal recovery. The mechanism explaining the fluorescent signal recovery upon the addition of proteins having different size and charge are displayed in **Figure 4.21**.

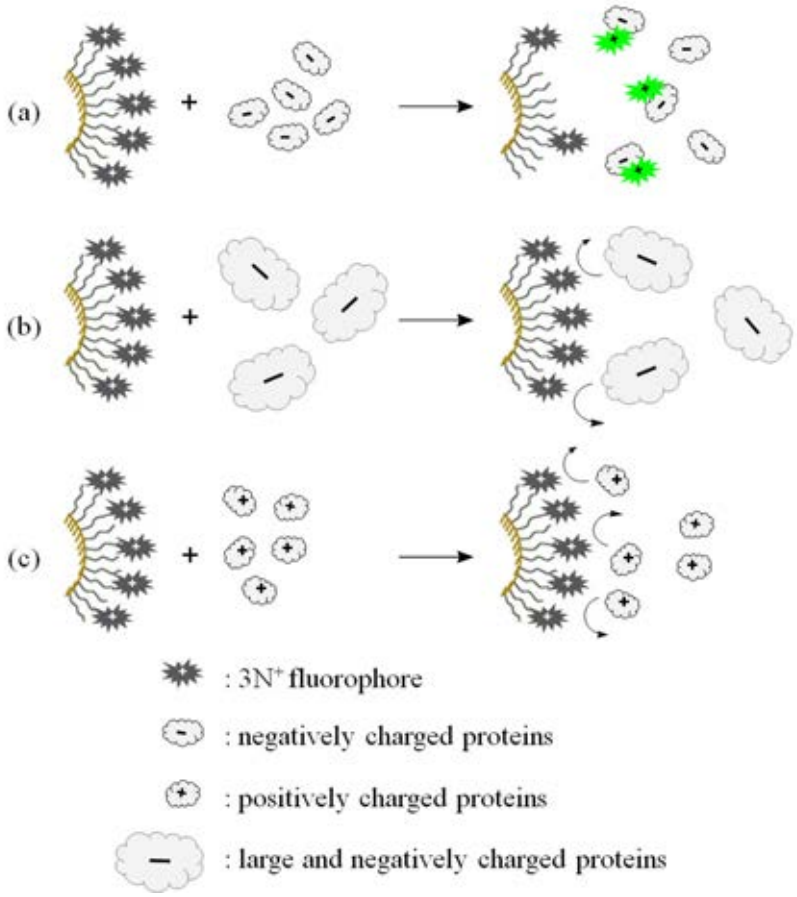


**Figure 4.21** Schematic representation of mechanism explaining the fluorescent signal recovery upon the addition of proteins having different size and charge.

In the case of Lys, a relatively small and positively charged protein, it was found that the signal recovery did not happen. This may be attributed to the repulsive forces between Lys and the $3N^+$ fluorophore. In fact, further quenching was also observed as can be realized from the negative responses of the signal. We describe the decreasing of fluorescent signal as a result of additional quenching of excess $3N^+$ fluorophore in the solution. This is likely possible given that it was demonstrated earlier in **Figure 4.15** that the $3N^+$ fluorophore was slightly quenched by proteins.

Although the results demonstrated in **Figure 4.20** suggested that the developed sensing platform using the PNIPAM-AuNPs in combination with $3N^+$ fluorophore was applicable for protein detection, the fact that the changes in fluorescence response ($\Delta I/I_0$) were determined from the maximum emission intensity independent of the wavelength was not intuitively accurate. Such estimation also ruled out the possibility that the wavelength of the emission maxima may be shifted upon protein addition which was found to be the case in some systems. For more accuracy, the whole spectra obtained before and after adding proteins were taken into consideration when performing subtraction. As can be seen in **Figure 4.22**, the subtracted spectra of each protein apparently exhibited different characteristic. The intensity values in every wavelength (400-600nm) of spectra were used to identify each protein.

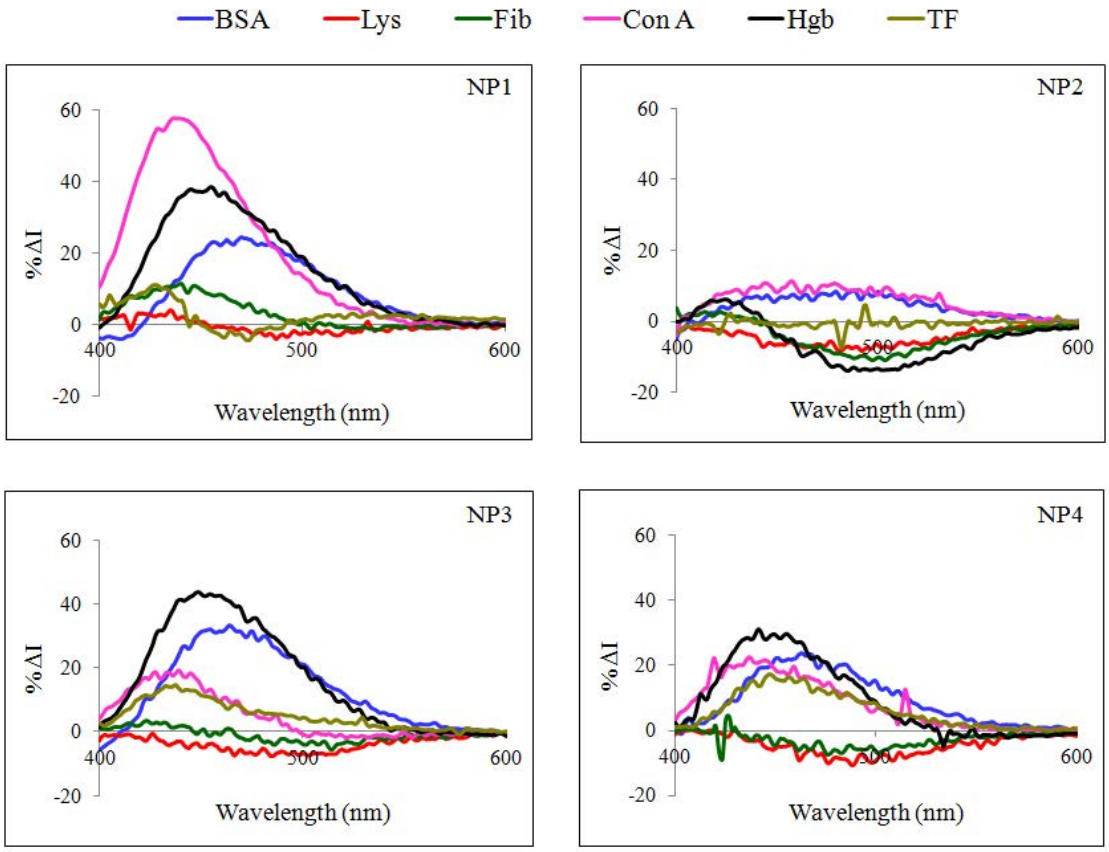


**Figure 4.22** Characteristic emission spectra of $3N^+$ fluorophore in the presence of PNIPAM-AuNPs for each type of proteins in PBS (obtained by the subtraction of spectra before and after protein addition).

Although the histogram plot (**Figure 4.18** and **Figure 4.20**) and characteristic spectrum (**Figure 4.22**) already showed different patterns of the fluorescent responses toward each protein analyte, discrimination of these proteins based on this multi-dimensional data set (5 AuNPs × 6 proteins × 6 replicates) was further simplified using multivariate statistical analyses. In this study, principal component analysis (PCA) was used to transform the data set of fluorescent intensity differences (%ΔI) into principle component (PC) scores [67]. Based on the data similarity, a two dimension PCA score plot suitably generated six clusters of PC scores corresponding to six types of proteins without knowing which data belong to same group indicating an encouraging level of protein classification (**Figure 4.23**).

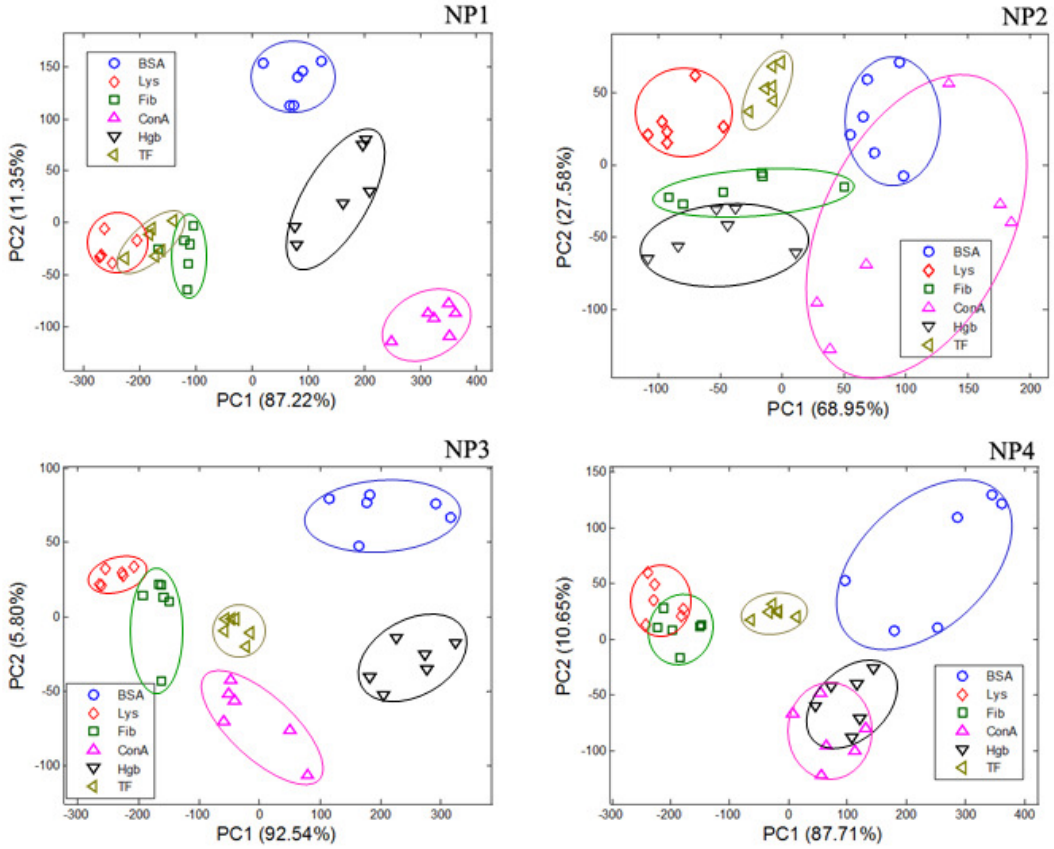


**Figure 4.23** PCA score plot of %ΔI data set obtained from 6 replicates of 6 proteins including fluorescence responses of $3N^+$ fluorophore using NP1, NP2, NP3, and NP4.

To quantify the classification accuracy, linear discriminant analysis (LDA) [61], was applied on the PC scores to cross-validate the discriminating ability using leave-one-out technique. After PCA/LDA routines performed on the data by using each type of AuNPs (NP1-NP4), the results showed that the data which used NP3 gave the highest classification accuracy of 97.22% (**Table 4.5**).

**Table 4.5** Percent correctly classified of each type of AuNPs obtained from LDA cross validation.

| Type of AuNPs | LDA cross validation (% correctly classified) |
|---|---|
| NP1 | 91.67 |
| NP2 | 75.00 |
| NP3 | 97.22 |
| NP4 | 66.67 |
| NP1 + NP2 | 94.44 |
| NP1 + NP3 | 94.44 |
| NP1 + NP4 | 100.00 |

The data obtained implied that the aggregation of PNIPAM layer induced by thermal treatment (NP2 and NP4) may deteriorate the efficiency of protein classification. However, we found that the 100% of classification accuracy can be obtained by combining NP1 data set with NP4 data set. The PCA score plot of NP1 associated with NP4 is shown in **Figure 4.24**. These results strongly indicate the high potential of the developed sensing platform given that proteins can be identified with 100% accuracy by using only two types of PNIPAM-AuNPs.

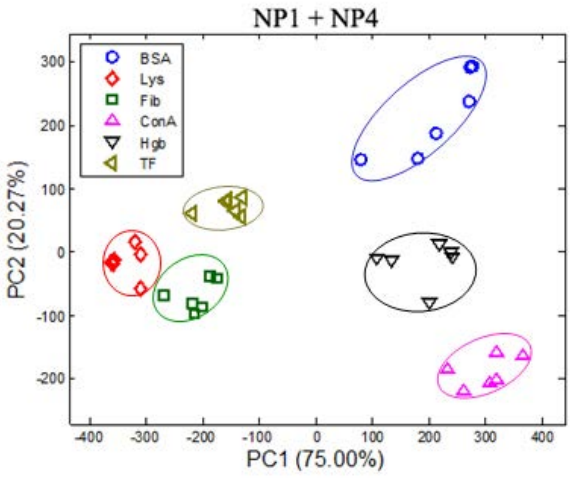


**Figure 4.24** PCA score plot obtained from the mixing of data set of NP1 and NP4.

# CHAPTER V

# CONCLUSION AND SUGGESTIONS

This investigation has demonstrated that the thermoresponsive AuNPs can be prepared by using citrate-stabilized AuNPs grafted with PNIPAM-SH synthesized via RAFT polymerization. The thickness of AuNPs shell depended on the PNIPAM-SH molecular weight. The prepared PNIPAM-AuNPs have a spherical morphology and uniform size distribution. The particles in aqueous solution exhibited a change of color from red to purple when the solution was heated to 40 °C due to the thermoresponsive behavior of PNIPAM on the AuNPs surface.

For the detection of proteins, PNIPAM-AuNPs having different characteristic can be simply generated by the variation of PNIPAM molecular weight and conformation. Based upon the concept of fluorescence quenching of fluorophore, NP1-NP4 possessed different quenching efficiency with $3N^+$ fluorophore. After adding protein, the fluorescence signal of $3N^+$ fluorophore can be recovered. The different pattern of fluorescent signal recovery which is varied with the types of both proteins and PNIPAM-AuNPs can be used to generate an array-based protein classification Based on LDA analysis, a 100% accuracy of protein classification can be obtained using a combination of NP1 data set and NP4 data set. The results have suggested that an array-based sensing platform based on chemical nose approach can be developed from PNIPAM-AuNPs.

For future work, it would be very challenging to explore the possibility of identifying the quantity of protein as well as a specific protein in multicomponent samples having a combination of known proteins.

# REFERENCES


[1] Ishii, T., Otsuka, H., Kataoka, K., and Nagasaki, Y. Preparation of functionally PEGylated gold nanoparticles with narrow distribution through autoreduction of auric cation by alpha-biotinyl-PEG-block-poly(2-(*N,N*-dimethylamino)ethyl methacrylate). Langmuir 20 (2004) : 561-564.

[2] Mirkin, C.A., Letsinger, R.L., Mucic, R.C., and Storhoff, J J. A DNA-based method for rationally assembling nanoparticles into macroscopic materials. Nature 382 (1996) : 607-609.

[3] Storhoff, J.J., Lazarides, A.A., Mucic, R.C., Mirkin, C.A., Letsinger, R.L., and Schatz, G.C. What controls the optical properties of DNA-linked gold nanoparticle assemblies. Journal of the American Chemical Society 122 (2000) : 4640-4650.

[4] Kratz, K., Hellweg, T., and Eimer, W. Structural changes in PNIPAM microgel particles as seen by SANS, DLS, and EM techniques. Polymer 42 (2001) : 6631-6639.

[5] Convertine, A.J., Ayres, N., Scales, C.W., Lowe, A.B., and McCormick, C.L. Facile, controlled, room-temperature RAFT polymerization of *N*-isopropylacrylamide. Biomacromolecules 5 (2004) : 1177-1180.

[6] Ganachaud, F., Monteiro, M.J., Gilbert, R.G., Dourges, M.A., Thang, S.H., and Rizzardo, E. Molecular weight characterization of poly(*N*-isopropylacrylamide) prepared by living free-radical polymerization. Macromolecules 33 (2000) : 6738-6745.

[7] Kujawa, P., and others. Impact of end-group association and main-chain hydration on the thermosensitive properties of hydrophobically modified telechelic poly(N-isopropylacrylamides) in water. Macromolecules 39 (2006) : 341-348.

[8] Ray, B., and others. Synthesis of isotactic poly(*N*-isopropylacrylamide) by RAFT polymerization in the presence of Lewis acid. Macromolecules 36 (2003) : 543-545.

[9] Schilli, C., Lanzendorfer, M.G., and Muller, A.H.E. Benzyl and cumyl dithiocarbamates as chain transfer agent in the RAFT polymerization of N-isopropylacrylamide. In situ FT-NIR and MALDI-TOF MS investigation. Macromolecules 35 (2002) : 6819-6827.

[10] Zhu. M.Q., Wang, L.Q., Exarhos, G.J., and Li, A.D.Q. Thermosensitive Gold Nanoparticles. Journal of the American Chemical Society 126 (2004) : 2656-2657.

[11] Raula, J., and others. Synthesis of gold nanoparticles grafted with a thermoresponsive polymer by surface-induced reversible-addition-fragmentation chain-transfer polymerization. Langmuir 19 (2003) : 3499-3504.

[12] Shan, J., Chen, J., Nuopponen, M., and Tenhu, H. Two phase transitions of poly(N-isopropylacrylamide) brushes bound to gold nanoparticles. Langmuir 20 (2004) : 4671-4676.

[13] Shan, J., Nuopponen, M., Jiang, H., Kauppinen, E., and Tenhu, H. Preparation of poly(*N*-isopropylacrylamide)-monolayer-protected gold clusters: Synthesis methods, core size, and thickness of monolayer. Macromolecules 36 (2003) : 4526-4533.

[14] De, M., and others. Sensing of proteins in human serum using conjugates of nanoparticles and green fluorescent protein. Nature Chemistry 1 (2009) : 461-465.

[15] Whitesides, G.M. The 'right' size in nanobiotechnology. Nature Biotechnology 21 (2003) : 1161-1165.

[16] http://twins.twmu.ac.jp/first/en/technology_base.html

[17] Basu, N., Bhattacharya, R., and Mukherjee, P. Protein-mediated autoreduction of gold salts to gold nanoparticles. Biomedical Materials 3 (2008).

[18] Vanden Bout, D.A. Metal Nanoparticles: Synthesis, Characterization, and Applications. Journal of the American Chemical Society 124 (2002) : 7874-7875.

[19] Kreibig, U., and Vollmer, M. Optical properties of metal clusters. Springer, 1995.

[20] Daniel, M.C., and Astruc, D. Gold nanoparticles: Assembly, supramolecular chemistry, quantum-size-related properties, and applications toward biology, catalysis, and nanotechnology. Chemical Reviews 104 (2004) : 293-346.

[21] Haick, H. Chemical sensors based on molecularly modified metallic nanoparticles. Journal of Physics D-Applied Physics 40 (2007) : 7173-7186.

[22] Radwan, S.H., and Azzazy, H.M.E. Gold nanoparticles for molecular diagnostics. Expert Review of Molecular Diagnostics 9 (2009) : 511-524.

[23] Zayats, M., Baron, R., Popov, I., and Willner, I. Biocatalytic growth of Au nanoparticles: From mechanistic aspects to biosensors design. Nano Letters 5 (2005) : 21-25.

[24] Yonezawa, T., and Kunitake, T. Practical preparation of anionic mercapto ligand-stabilized gold nanoparticles and their immobilization. Colloids and Surfaces a-Physicochemical and Engineering Aspect*s* 149 (1999) : 193-199.

[25] Corbierre, M.K., Cameron, N.S., and Lennox, R.B. Polymer-stabilized gold nanoparticles with high grafting densities. Langmuir 20 (2004) : 2867-2873.

[26] Du, B.Y., Zhao, B., Tao, P.J., Yin, K.Z., Lei, P., and Wang, Q. Amphiphilic multiblock copolymer stabilized Au nanoparticles. Colloids and Surfaces a-Physicochemical and Engineering Aspects 317 (2008) : 194-205.

[27] Kim, D.J., Kang, S.M., Kong, B., Kim, W.J., Paik, H.J., Choi, H., and Choi, I.S. Formation of thermoresponsive gold nanoparticle/PNIPAAm hybrids by surface-initiated, atom transfer radical polymerization in aqueous media. Macromolecular Chemistry and Physics 206 (2005) : 1941-1946.

[28] Nuss, S., Bottcher, H., Wurm, H., and Hallensleben, M.L. Gold nanoparticles with covalently attached polymer chains. Angewandte Chemie-International Edition 40 (2001) : 4016.

[29] Ohno, K., Koh, K., Tsujii, Y., and Fukuda, T. Synthesis of gold nanoparticles coated with well-defined, high-density polymer brushes by surface-initiated living radical polymerization. Macromolecules 35 (2002) : 8989-8993.

[30] Mandal, T.K., Fleming, M.S., and Walt, D.R. Preparation of polymer coated gold nanoparticles by surface-confined living radical polymerization at ambient temperature. Nano Letters 2 (2002) : 3-7.

[31] Li, D.X., He, Q., Cui, Y., and Li, J.B. Fabrication of pH-responsive nanocomposites of gold nanoparticles/poly(4-vinylpyridine). Chemistry of Materials 19 (2007) : 412-417.

[32] Yoon, K.R., Ramaraj, B., Lee, S.M., and Kim, D.P. Surface initiated-atom transfer radical polymerization of a sugar methacrylate on gold nanoparticles. Surface and Interface Analysis *40* (2008) : 1139-1143.

[33] Huang, H.M., Chang, C.Y., Liu, I.C., Tsai, H.C., Lai, M.K., and Tsiang, R.C.C. Synthesis of gold nanocomposite via chernisorption of gold nanoparticles with poly(p-methyl styrene) containing multiple bonding groups on the chain side. Journal of Polymer Science Part a-Polymer Chemistry 43 (2005) : 4710-4720.

[34] Hussain, I., and others. Size-controlled synthesis of near-monodisperse gold nanoparticles in the 1-4 nm range using polymeric stabilizers. Journal of the American Chemical Society 127 (2005) : 16398-16399.

[35] Kim, B.J., Bang, J., Hawker, C.J., and Kramer, E.J. Effect of areal chain density on the location of polymer-modified gold nanoparticles in a block copolymer template. Macromolecules 39 (2006) : 4108-4114.

[36] Suzuki, D., and Kawaguchi, H. Modification of gold nanoparticle composite nanostructures using thermosensitive core-shell particles as a template. Langmuir 21 (2005) : 8175-8179.

[37] Cui, Y., Tao, C., Zheng, S.P., He, Q., Ai, S.F., and Li, J.B. Synthesis of thermosensitive PNIPAM-co-MBAA nanotubes by atom transfer radical polymerization within a porous membrane. Macromolecular Rapid Communications 26 (2005) : 1552-1556.

[38] Gil, E.S., and Hudson, S.M. Stimuli-reponsive polymers and their bioconjugates. *Progress in Polymer Science* 29 (2004) : 1173-1222.

[39] Hu, Z.B., Chen, Y.Y., Wang, C.J., Zheng, Y.D., and Li, Y. Polymer gels with engineered environmentally responsive surface patterns. Nature 393 (1998) : 149-152.

[40] Schilli, C.M., and others. A new double-responsive block copolymer synthesized via RAFT polymerization: Poly(N-isopropylacrylamide)-block-poly(acrylic acid). Macromolecules 37 (2004) : 7861-7866.

[41] Bohrisch, J., Wendler, U., and Jaeger, W. Controlled radical polymerization of 4-vinylpyridine. Macromolecular Rapid Communications 18 (1997) : 975-982.

[42] Fischer, A., Brembilla, A., and Lochon, P. Nitroxide-mediated radical polymerization of 4-vinylpyridine: Study of the pseudo-living character of the reaction and influence of temperature and nitroxide concentration. Macromolecules 32 (1999) : 6069-6072.

[43] Ista, L.K., Mendez, S., Perez-Luna, V.H., and Lopez, G.P. Synthesis of poly(*N*-isopropylacrylamide) on initiator-modified self-assembled monolayers. Langmuir 17 (2001) : 2552-2555.

[44] Mika, A.M., and Childs, R.F. Acid/base properties of poly(4-vinylpyridine) anchored within microporous membranes. Journal of Membrane Science 152 (1999) : 129-140.

[45] Wang, X.H., and Wu, C. Light-scattering study of coil-to-globule transition of a poly(*N*-isopropylacrylamide) chain in deuterated water. Macromolecules 32 (1999) : 4299-4301.

[46] Wu, C., and Zhou, S.Q. Thermodinamically stable globule state of a single poly(*N*-isopropylacrylamide) chain in water. Macromolecules 28 (1995) : 5388-5390.

[47] Zhang, J., and Pelton, R. The dynamic behavior of poly(*N*-isopropylacrylamide) at the air/water interface. Colloids and Surfaces a-Physicochemical and Engineering Aspects 156 (1999) : 111-122.

[48] Yusa, S.I., and others. Salt effect on the heat-induced association Behavior of gold nanoparticles coated with Poly(*N*-isopropylacrylamide) prepared via reversible addition - Fragmentation chain transfer (RAFT) radical polymerization. Langmuir 23 (2007) : 12842-12848.

[49] Chakraborty, S., Bishnoi, S.W., and Perez-Luna, V.H. Gold Nanoparticles with Poly(*N*-isopropylacrylamide) Formed via Surface Initiated Atom Transfer Free Radical Polymerization Exhibit Unusually Slow Aggregation Kinetics. Journal of Physical Chemistry *C* 114 (2010) : 5947-5955.

[50] Arai, R., and others. Demonstration of a homogeneous noncompetitive immunoassay based on bioluminescence resonance energy transfer. Analytical Biochemistry 289 (2001) : 77-81.

[51] Sanchez-Martinez, M.L., Aguilar-Caballos, M.P., and Gomez-Hens, A. Homogeneous immunoassay for soy protein determination in food samples using gold nanoparticles as labels and light scattering detection. Analytica Chimica Acta 636 (2009) : 58-62.

[52] Templeton, A.C., Wuelfing, W.P., and Murray, R.W. Monolayer-Protected Cluster Molecules. Accounts of Chemical Research 33 (1999) : 27-36.

[53] Du, B.A., Li, Z.P., and Cheng, Y.Q. Homogeneous immunoassay based on aggregation of antibody-functionalized gold nanoparticles coupled with light scattering detection, Talanta 75 (2008) 959-964.

[54] Chen, J.W., Lei, Y., Liu, X.J., Jiang, J.H., Shen, G.L., and Yu, R.Q. Immunoassay using surface-enhanced Raman scattering based on aggregation of reporter-labeled immunogold nanoparticles. Analytical and Bioanalytical Chemistry 392 (2008) : 187-193.

[55] Dulkeith, E., Ringler, M., Klar, T.A., Feldmann, J., Javier, A.M., and Parak, W.J. Gold nanoparticles quench fluorescence by phase induced radiative rate suppression. Nano Letters 5 (2005) : 585-589.

[56] Miranda, O.R., Creran, B., and Rotello, V.M. Array-based sensing with nanoparticles: 'Chemical noses' for sensing biomolecules and cell surfaces. Current Opinion in Chemical Biology 14 (2010) : 728-736.

[57] You, C.C., and others. Detection and identification of proteins using nanoparticle-fluorescent polymer 'chemical nose' sensors. Nature Nanotechnology 2 (2007) : 318-323.

[58] De, M., You, C.C., Srivastava, S., and Rotello, V.M. Biomimetic interactions of proteins with functionalized nanoparticles: A thermodynamic study. Journal of the American Chemical Society 129 (2007) : 10747-10753.

[59] Saha, K., Agasti, S.S, Kim, C., Li, X., and Rotello, V.M. Gold Nanoparticles in Chemical and Biological Sensing. Chemical Reviews (2012).

[60] Phillips, R.L., Miranda, O.R., You, C.C., Rotello, V.M., and Bunz, U.H.F. Rapid and efficient identification of bacteria using gold-nanoparticle - Poly(para-phenyleneethynylene) constructs. Angewandte Chemie-International Edition 47 (2008) : 2590-2594.

[61] Hayat, A. Colloidal gold: principles, methods, and applications. Journal of Anatomy 176 (1989) : 215-216.

[62] Niamnont, N., Mungkarndee,R., Techakriengkrai, I., Rashatasakhon, P., and Sukwattanasinitt, M. Protein discrimination by fluorescent sensor array constituted of variously charged dendritic phenylene-ethynylene fluorophores. Biosensors and Bioelectronics 26 (2010) : 863-867.

[63] Nakayama, M., and Okano, T. Polymer terminal group effects on properties of thermoresponsive polymeric micelles with controlled outer-shell chain lengths. Biomacromolecules 6 (2005) : 2320-2327.

[64] Fang, Z., and Kennedy, J.P. Novel block ionomers II. Synthesis and characterization of polyisobutylene-based block cationomers. Journal of Polymer Science Part a-Polymer Chemistry 40 (2002) : 3679-3691.

[65] Scales, C.W., Convertine, A.J., and McCormick, C.L. Room-temperature polymerization of *N*-isopropylacrylamide via RAFT and subsequent conjugation of fluorescent labels. Abstracts of Papers of the American Chemical Society 230 (2005) : 4233-4234.

[66] Paik, W.K., Han, S.B., Shin, W., and Kim, Y.S. Adsorption of carboxylic acids on gold by anodic reaction. Langmuir 19 (2003) : 4211-4216.

[67] Poulli, K.I., Mousdis, G.A., and Georgiou, C.A. Classification of edible and lampante virgin olive oil based on synchronous fluorescence and total luminescence spectroscopy. Analytica Chimica Acta 542 (2005) : 151-156.

# APPENDIX

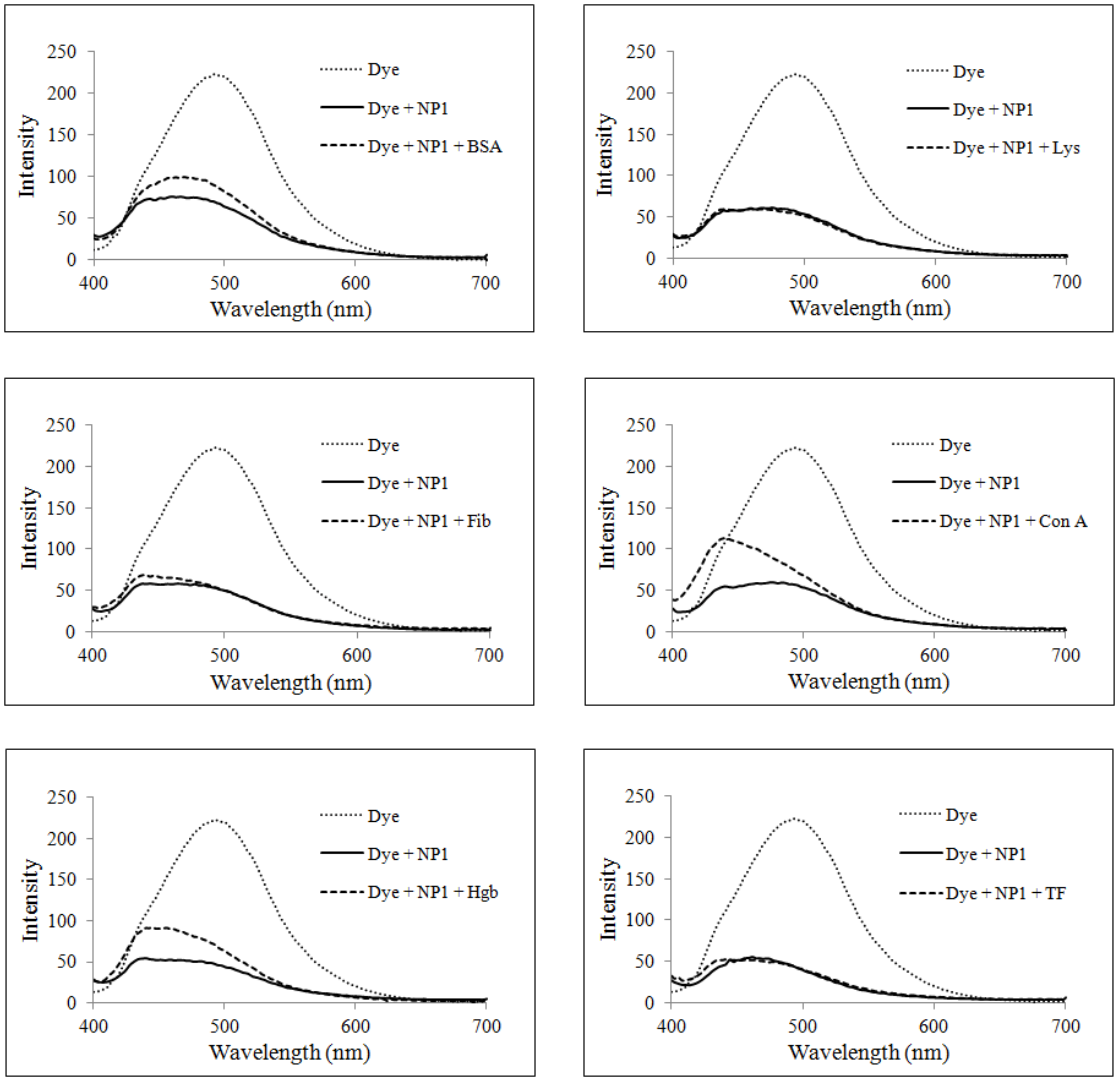


**Figure A.1** Fluorescence emission spectra demonstrating quenching behavior of $3N^+$ fluorophore in the presence of NP1 before and after protein addition.

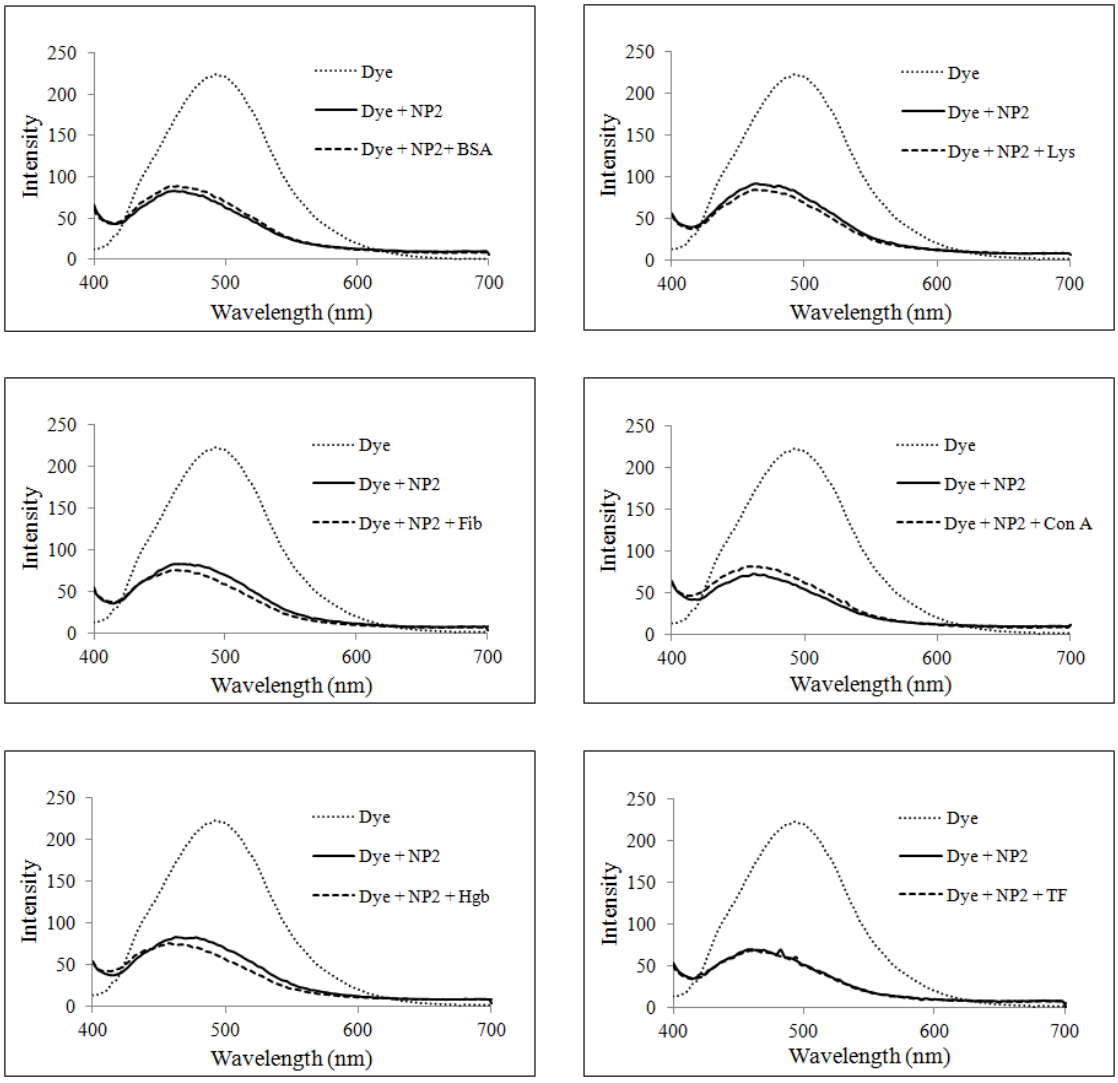


**Figure A.2** Fluorescence emission spectra demonstrating quenching behavior of $3N^+$ fluorophore in the presence of NP2 before and after protein addition.

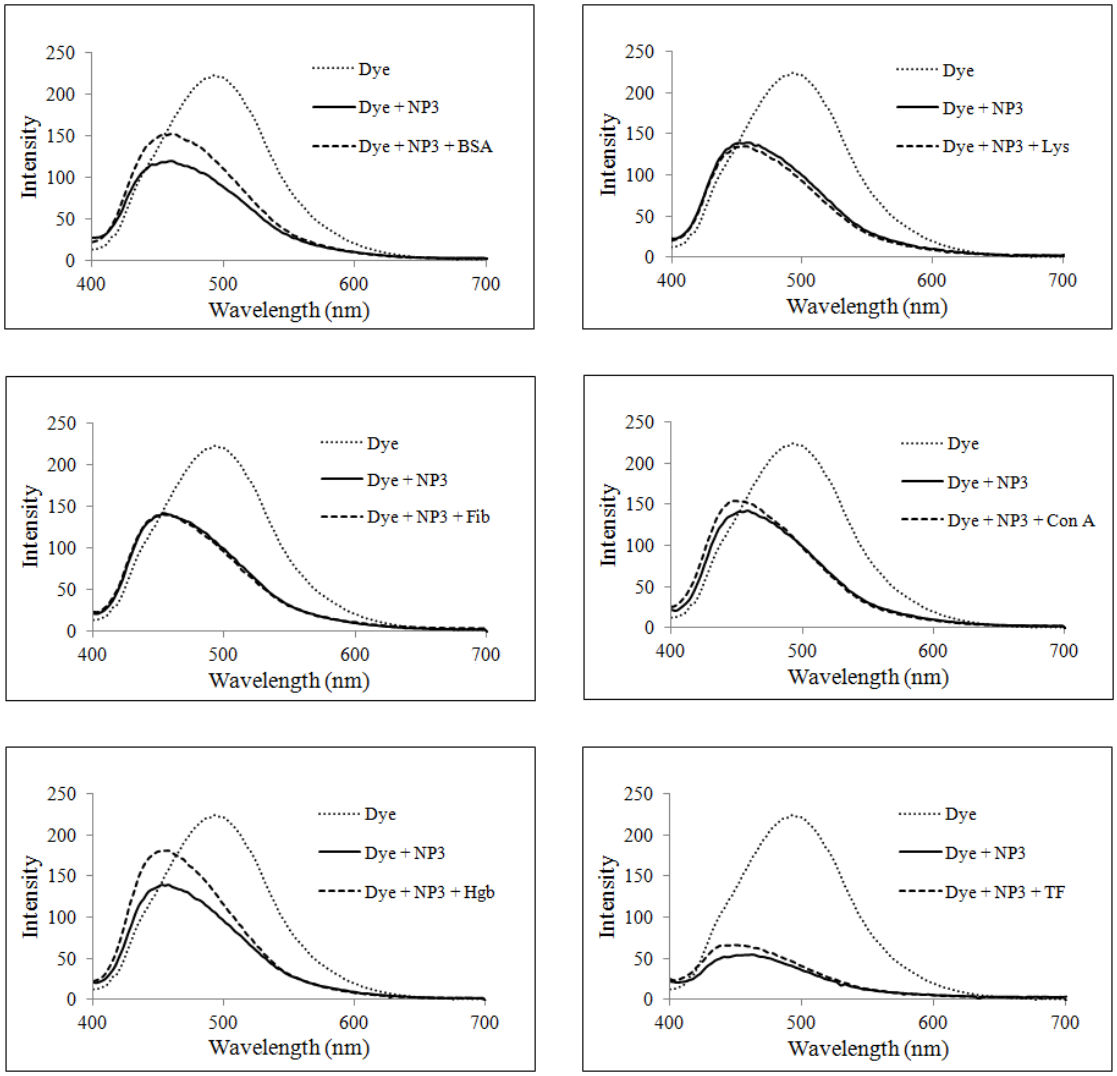


**Figure A.3** Fluorescence emission spectra demonstrating quenching behavior of $3N^+$ fluorophore in the presence of NP3 before and after protein addition.

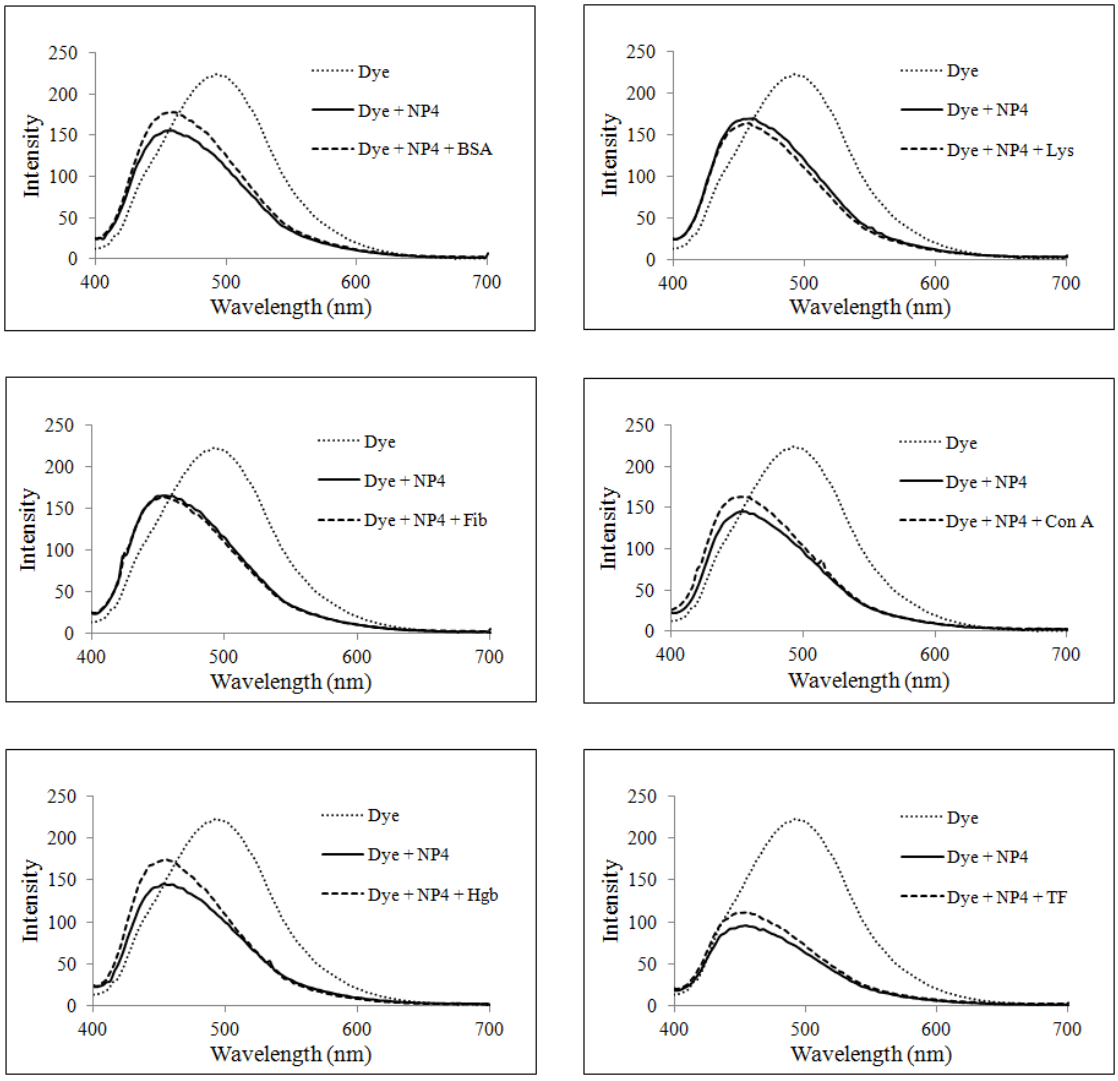


**Figure A.4** Fluorescence emission spectra demonstrating quenching behavior of $3N^+$ fluorophore in the presence of NP4 before and after protein addition.

# VITAE

Miss Keerati Kusolkamabot was born in Bangkok, Thailand, on July 17th, 1985. She received a Bachelor Degree of Science in Chemistry from the Faculty of Science, King Mongkut's University of Technology North Bangkok, Bangkok in 2009. In the same year, she started as a Master Degree student with a major in Program of Petrochemistry and Polymer Science, Faculty of Science, Chulalongkorn University and completed the program in May, 2012.

**Proceedindings:**

October 2011 Oral presentation in The 2nd Polymer Conference of Thailand (PCT-2), Chulabhorn Research Institute, Bangkok, Thailand.

**Presentation in Conference:**

January 2012 Poster presentation in The 6th Pure and Applied Chemistry International Conference (PACCON2012). Empress Hotel, Chiang Mai, Thailand.